J. Fluid Mech. (2000), *vol.* 422, *pp.* 91–123. Printed in the United Kingdom

© 2000 Cambridge University Press

Pressure–strain correlation modelling of complex turbulent flows

By SHARATH S. GIRIMAJI

Aerospace Engineering Department, Texas A & M University, College Station, TX 77843-3141, USA

(Received 8 December 1997 and in revised form 24 April 2000)

A methodology for deriving a pressure–strain correlation model with variable coefficients is developed. The methodology is based on two important premises: (i) the extreme states of turbulence – the rapid distortion and equilibrium limits – are more amenable to mathematically rigorous modelling because of significant simplifications not possible at other states; and (ii) the models of the extreme states collectively contain all of the relevant physics so that models for any intermediate state can be obtained by suitable interpolation. A pressure–strain model of the standard form is considered and the coefficients are determined from linear analysis in the rapid distortion limit and from a fixed point analysis in the equilibrium limit. The model coefficients, which depend on the mean deformation and turbulence state, vary from flow to flow in a manner consistent with Navier–Stokes physics.

The exact causal relationship between the model coefficients and the model's equilibrium behaviour is established by fixed point analysis performed using representation theory. Then, the equilibrium values of the model coefficients are chosen to yield the observed equilibrium behaviour. The values of the model coefficients in the rapid distortion limit are determined by enforcing consistency with the Crow constraint. The new variable-coefficient model reduces to the traditional constant-coefficient model in strain-dominated turbulent flows near equilibrium. The model performance in benchmark turbulent flows, in which the traditional models have been calibrated extensively, is preserved intact. The new model is significantly different from the traditional one in mean vorticity-dominated and non-equilibrium turbulence. These two important classes of flows, in which traditional models fail, are successfully captured by the new model.

1. Introduction

The linear pressure–strain correlation model, of the form popularized by Launder, Reece & Rodi (1975) (LRR), continues to be the popular choice for turbulence calculations at the second-moment closure level. The longevity of this model is due equally to its success in a variety of important benchmark flows as it is to its simplicity. Benchmark flows have typically been important engineering flows such as boundary layers, plane jets, mixing layers and equilibrium states of homogeneous strain-dominated turbulence such as plane shear, plane strain and axisymmetric expansion/contraction. Over the last several years there have been important improvements (e.g. Speziale, Sarkar & Gatski 1991 (SSG); Ristorcelli, Lumley & Abid 1995) resulting in better predictions over a wider range of flows, especially rotating flows. However, it has been recently demonstrated by Blaisdell & Shariff (1996) (see also Kassinos & Reynolds

https://doi.org/10.1017/S0022112000001336 Published online by Cambridge University Press

1994) that these models generally perform very poorly in an important class of vorticity-dominated flows called the elliptic streamline flows – these are homogeneous flows with constant mean strain and rotation rates. The flow is named after the elliptic shape of the mean streamlines when the magnitude of strain is lower than that of rotation rate or vorticity. The model computations are even qualitatively inconsistent with linear stability theory and direct numerical simulation (DNS) data for this class of flows. A second class of flows in which the standard pressure–strain correlation models are inadequate is non-equilibrium turbulent flows. These two classes of flows in which the models fail or perform poorly are encountered in many important engineering applications. Vorticity-dominated flows include many aeronautical flows such as trailing vortex, flap-edge vortex and leading-edge vortex flows. Highly-strained flows, such as flows with shock–turbulence interactions, are examples of non-equilibrium flows. Clearly, there is a need for turbulence models that can compute these flows with a reasonable degree of accuracy and confidence.

The failure of the traditional pressure-correlation models in these flows is generally presumed to be a natural consequence of the simplicity of the model form and the modelling assumptions. In turbulent flows dominated by rotation, Kassinos & Reynolds (1994) find that additional tensors are needed to accurately describe the state of turbulence. Their analysis results in a more complex model formulation based on the structure-function tensor. Van Slooten & Pope (1997) have derived a Langevin-particle equivalent of the structure-function model. These more advanced models perform better than the standard Reynolds stress closure models for elliptic flows at the expense of added computational effort. Due to their inherent complexity and lack of validation over a wide range of practical flows, these advanced models are not yet useful design tools.

Modelling premise and objective. The premise of this paper is that the traditional pressure–strain correlation model form is quite adequate: the poor performance in complex (elliptic and non-equilibrium) flows may be due more to the sub-optimal choice of model coefficients than to a fundamental flaw in the modelling methodology. In fact, the traditional form of the pressure–strain model has a rigorous mathematical justification (Speziale *et al.* 1991) in high-Reynolds-number equilibrium turbulence with strong locality and negligible history effects. Under these conditions, the model coefficients could be scalar functions of the invariants of the strain rate, rotation rate and Reynolds stress anisotropy. With notable exceptions (e.g. Ristorcelli *et al.* 1995), the pressure–strain correlation models in the literature typically assign constant values to the model coefficients. Although these models perform well in calibration flows, they are much less accurate in flows where the imposed strain and rotation rates differ from the calibration conditions. Since most of the calibration is based on strain-dominated flows, it should come as no surprise that these models predict the vorticity-dominated elliptic flows poorly. To capture the behaviour of complex flows, the model coefficients must be functions of the imposed deformation rate and the state of turbulence.

In this paper, we initiate the development of a new pressure–strain correlation model with 'optimal' variable coefficients. These model coefficients change, in accordance with Navier–Stokes physics, from flow to flow in a manner that highlights the appropriate physics. The proposed model yields excellent agreement with data for a variety of complex flows and reduces to the well-tested traditional model in standard benchmark cases.

The analysis leading to the development of the new pressure–strain correlation model requires the specification of the dissipation rate. In keeping with the theme of

https://doi.org/10.1017/S0022112000001336 Published online by Cambridge University Press

this paper, we use a model dissipation equation of the time-tested standard form. Our analysis can also be used to develop a variable-coefficient dissipation model equation of the standard form, but that has been deferred to the future.

1.1. *Modelling methodology*

The phenomenon of turbulence is a complex interaction between the linear production mechanism, the nonlinear spectral cascade and the viscous dissipation of turbulent kinetic energy. The relative importance of each mechanism depends on the state of turbulence and the mean deformation. The three limiting states of turbulence – rapid distortion, equilibrium and decay – represent the extremes of the physics of turbulence. In the rapid distortion state, only the linear physics is relevant. At the other extreme, in the decaying isotropic state, only the nonlinear cascade and dissipation effects are present. In the equilibrium state of turbulence, both linear and nonlinear mechanisms are important. In order to build an 'optimal' turbulence model, which incorporates all the above features, a two-step methodology is proposed.

In the first step, pressure–strain correlation models for each of the extreme states are developed separately. As each extreme state is amenable to special analysis, the individual models (read model coefficients) can be developed with a degree of mathematical rigour impossible in arbitrary states. The intermediate states of turbulence are more difficult to analyse because of the complex interplay among the various competing processes. However, to date, there is no evidence of loss of regularity in the physics of turbulence between the rapid distortion state and equilibrium. The turbulence physics appears to vary smoothly between the different extremes. This means that the individual models of the extreme states can be expected, collectively, to contain all of the important physics. A matched asymptotic interpolation between the extreme states appears fully justified. In the second step, we propose that the pressure–strain correlation model for an arbitrary state of turbulence be determined by interpolation between the models of extreme states using a suitable state parameter. The interpolation scheme proposed herein must be regarded as only an initial, yet important, effort towards fully understanding and modelling the intermediate states of turbulence.

The pressure–strain correlation model cannot be developed completely independent of the dissipation model. The two-step modelling methodology described above can also be used to develop a variable-coefficient dissipation model of the standard form. A dissipation model equation with variable optimal coefficients may enjoy a greater degree of validity than its constant-coefficient counterpart.

Equilibrium turbulence. This state of turbulence which permits fixed point and bifurcation analyses is encountered in many fully developed engineering flows. Many aspects of turbulence in equilibrium are understood from laboratory and numerical experiments. Our objective is to construct a turbulence model that is consistent with observed behaviour. This calls for an intimate understanding of the connection between the model coefficients and predicted equilibrium behaviour. We perform fixed point and bifurcation analyses to establish, for the first time, the exact analytical relationship between the model's coefficients and its equilibrium behaviour. Once this connection is determined, the coefficients are chosen to yield the required equilibrium behaviour. The analyses indicate that in complex turbulent flows (with dominant rotation and/or strain effects), the equilibrium model coefficients must be functions of the mean flow deformation. The ratio of mean strain to total deformation, which we call the deformation parameter, emerges as the most significant metric of the mean flow deformation. This parameter goes to unity in purely strained flows and is

https://doi.org/10.1017/S0022112000001336 Published online by Cambridge University Press

zero in purely vortical flows. We note that fixed point analyses have been performed in different contexts by Abid & Speziale (1993) and Speziale & Mac Giolla Mhuiris (1989, 1990).

Rapid distortion limit. When the mean flow deformation rate is much larger than the turbulence strain rate, a linear analysis called the rapid distortion theory (RDT) is possible. We will specify the model coefficients in the rapidly distorted limit by requiring consistency with the RDT result of Crow (1968), the so-called Crow constraint. The pressure–strain model for moderately non-equilibrium turbulence is obtained by interpolating between the rapid distortion and equilibrium models using a parameter called the timescale ratio. This is the ratio between turbulent and mean flow strain rates and is the most significant scalar metric of the degree of departure from equilibrium. It goes to zero in the rapid distortion limit and to a known value in the equilibrium limit.

Decaying turbulence. In this limiting state, which is called the return-to-isotropy turbulence, the production mechanism is absent. Only a portion of the pressure–strain correlation, the slow part, is non-zero. Detailed consideration of the slow pressure–strain correlation is deferred to future work.

In this paper, we will consider the popular quasi-linear pressure–strain correlation model form (which includes all LRR-type models). Again, our principal objective is to evaluate the model coefficients to yield the highest degree of consistency possible with observed behaviour. In our model development, we will restrict ourselves to two-dimensional mean flows although the methodology itself is equally valid for other higher-order model forms and three-dimensional mean flows. The word 'complex' in the title of the paper refers to non-traditional combinations of mean strain and rotation, and flows far from equilibrium. The remainder of the paper is organized as follows. In § 2, we present the Reynolds stress closure equations. The fixed point and bifurcation analyses are given in § 3. The equilibrium pressure–strain correlation model is developed in § 4. In § 5, we propose a non-equilibrium modification to the model. Section 6 contains the results and discussion, and we conclude in § 7 with a summary.

2. Turbulence closure equations

In incompressible homogeneous turbulence subject to constant mean velocity gradients, the exact Reynolds stress transport equation in an inertial reference frame is given by

$$\frac{\mathrm{d}\overline{u_i u_j}}{\mathrm{d}t^*} = P_{ij} - \varepsilon_{ij} + \phi'_{ij}. \tag{1}$$

The terms in the above equation are, respectively, the time rate of change, production (P_{ij}), dissipation (ε_{ij}) and pressure–strain correlation (ϕ'_{ij}) of Reynolds stress:

$$P_{ij} = -\overline{u_i u_k}\frac{\partial U_j}{\partial x_k} - \overline{u_j u_k}\frac{\partial U_i}{\partial x_k}, \quad \varepsilon_{ij} = 2\nu\overline{\frac{\partial u_i}{\partial x_k}\frac{\partial u_j}{\partial x_k}}, \quad \phi'_{ij} = \overline{p\left(\frac{\partial u_i}{\partial x_j} + \frac{\partial u_j}{\partial x_i}\right)}. \tag{2}$$

The production and dissipation rate of turbulent kinetic energy are, respectively, $P = \frac{1}{2}P_{ii}$ and $\varepsilon = \frac{1}{2}\varepsilon_{ii}$. The dissipation is decomposed into its deviatoric and isotropic parts:

$$\varepsilon_{ij} = d_{ij} + \tfrac{2}{3}\varepsilon\delta_{ij}. \tag{3}$$

https://doi.org/10.1017/S0022112000001336 Published online by Cambridge University Press

The deviatoric part of dissipation is combined with the pressure–strain correlation and the two are modelled together:

$$\phi_{ij} = \phi'_{ij} + d_{ij}. \tag{4}$$

In high-Reynolds-number turbulence, the dissipation is isotropic ($d_{ij} = 0$) and, for all practical purposes, ϕ_{ij} is the pressure–strain correlation. Closure models are now needed for the pressure–strain correlation (ϕ_{ij}) and dissipation rate (ε).

As mentioned in the Introduction, we will focus on the quasi-linear pressure–strain correlation model form (following the SSG notation):

$$\begin{aligned}\phi_{ij} = -(C_1^0\varepsilon + C_1^1 P)b_{ij} + C_2 K S_{ij} + C_3 K(b_{ik}S^*_{jk} + b_{jk}S^*_{ik} - \tfrac{2}{3}b_{mn}S^*_{mn}\delta_{ij}) \\ + C_4 K(b_{ik}W^*_{jk} + b_{jk}W^*_{ik}),\end{aligned} \tag{5}$$

where the C are model coefficients and

$$S^*_{ij} = \frac{1}{2}\left(\frac{\partial U_i}{\partial x_j} + \frac{\partial U_j}{\partial x_i}\right), \quad W^*_{ij} = \frac{1}{2}\left(\frac{\partial U_i}{\partial x_j} - \frac{\partial U_j}{\partial x_i}\right), \quad K = \tfrac{1}{2}\overline{u_i u_i}, \quad b_{ij} = \frac{\overline{u_i u_j}}{2K} - \tfrac{1}{3}\delta_{ij}. \tag{6}$$

We choose this form of the pressure–strain model for two reasons. First, this form has mathematical justification in high-Reynolds-number near-equilibrium turbulent flows with a two-dimensional mean velocity field (Speziale *et al.* 1991). Second, this form is most frequently used in practical Reynolds stress closure calculations: it includes all linear-pressure strain models (e.g. the LRR model); further, some of the nonlinear models (such as the SSG model) can also be reduced to this form near equilibrium. For the LRR model, the coefficients are

$$C_1^0 = 3.0, \quad C_1^1 = 0, \quad C_2 = 0.8, \quad C_3 = 1.75, \quad C_4 = 1.31. \tag{7}$$

A variant of the above model also given in LRR is

$$C_1^0 = 3.6, \quad C_1^1 = 0, \quad C_2 = 0.8, \quad C_3 = 1.2, \quad C_4 = 1.2. \tag{8}$$

For the quasi-linearized SSG model, the coefficients are

$$C_1^0 = 3.4, \quad C_1^1 = 1.8, \quad C_2 = 0.36, \quad C_3 = 1.25, \quad C_4 = 0.4. \tag{9}$$

In an important departure from many previous models, in this study the model coefficients are not assigned constant values, but are functions of the mean deformation and the state of turbulence:

$$C_\alpha = C_\alpha(b_{ij}, S_{ij}, W_{ij}, K, \varepsilon). \tag{10}$$

The anisotropy evolution equation can be derived from the Reynolds stress equation:

$$\begin{aligned}\frac{\mathrm{d}b_{ij}}{\mathrm{d}t^*} = -b_{ij}\left(L_1^0\frac{\varepsilon}{K} - L_1^1 b_{mn}S^*_{mn}\right) + L_2 S^*_{ij} + L_3(b_{ik}S^*_{jk} + b_{jk}S^*_{ik} - \tfrac{2}{3}b_{lm}S^*_{lm}\delta_{ij}) \\ + L_4(b_{ik}W^*_{jk} + b_{jk}W^*_{ik}).\end{aligned} \tag{11}$$

In the above equation, the pressure–strain correlation model coefficients are redefined as

$$L_1^0 \equiv \frac{C_1^0}{2} - 1, \quad L_1^1 \equiv C_1^1 + 2, \quad L_2 \equiv \frac{C_2}{2} - \frac{2}{3}, \quad L_3 \equiv \frac{C_3}{2} - 1, \quad L_4 \equiv \frac{C_4}{2} - 1. \tag{12}$$

https://doi.org/10.1017/S0022112000001336 Published online by Cambridge University Press

The turbulent kinetic energy evolves according to

$$\frac{\mathrm{d}K}{\mathrm{d}t^*} = P - \varepsilon, \tag{13}$$

and the modelled evolution equation for dissipation is

$$\frac{\mathrm{d}\varepsilon}{\mathrm{d}t^*} = C_{e1}\frac{\varepsilon}{K}P - C_{e2}\frac{\varepsilon^2}{K}. \tag{14}$$

In the current analysis, C_{e1} and C_{e2} are arbitrary scalar functions of the state of turbulence and mean deformation invariants. In general, the dissipation rate model (with constant coefficients) represents a major weak link in turbulence modelling of complex flows. Its form and physical content deserve separate consideration which is not attempted here. More sophisticated dissipation models currently available seem to lack the general applicability of this simple model. A complete analysis with a more advanced dissipation equation will be attempted in the future.

Equations (11), (13) and (14) constitute the second-order closure equations in homogeneous turbulence. These equations can be non-dimensionalized using the norm of the velocity gradient tensor:

$$\eta = S^*_{ij}S^*_{ij} + W^*_{ij}W^*_{ij}. \tag{15}$$

The non-dimensional quantities are

$$S_{ij} = S^*_{ij}/\sqrt{\eta}, \quad W_{ij} = W^*_{ij}/\sqrt{\eta}, \quad \mathrm{d}t = \sqrt{\eta}\,\mathrm{d}t^*, \quad \omega = \varepsilon/(\sqrt{\eta}K), \tag{16}$$

where ω is the timescale ratio, the ratio of the turbulence to mean flow strain rates. In the above equations, symbols with and without asterisks denote dimensional and dimensionless quantities respectively. In dimensionless time, the anisotropy transport equation is

$$\frac{\mathrm{d}b_{ij}}{\mathrm{d}t} = -b_{ij}(L^0_1\omega - L^1_1 b_{mn}S_{mn}) + L_2S_{ij} + L_3(S_{ik}b_{kj} + b_{ik}S_{kj} - \tfrac{2}{3}b_{mn}S_{mn}\delta_{ij}) + L_4(W_{ik}b_{kj} - b_{ik}W_{kj}). \tag{17}$$

In dimensionless time, the anisotropy evolution depends only on: (i) the normalized mean strain and rotation and not on the magnitude of deformation (η); and (ii) the timescale ratio (ω) and not individually on kinetic energy and dissipation. The evolution equation for the timescale ratio, ω, is easily obtained from those for the turbulent kinetic energy and dissipation:

$$\frac{\mathrm{d}\omega}{\mathrm{d}t} = -2\omega(C_{e1} - 1)b_{mn}S_{mn} - (C_{e2} - 1)\omega^2. \tag{18}$$

The first term on the right-hand side of equation (18) represents the production of the timescale ratio and the second term represents its destruction.

The anisotropy equation (17) by itself is not autonomous as its behaviour is dependent on the relative timescale (ω). The anisotropy equation in conjunction with the equation for the relative timescale (18) form an autonomous nonlinear dynamical system which can be analysed. Therefore, the effects of the pressure–strain correlation and dissipation models are inseparable and the two must be modelled together to achieve the best results. The behaviour of this system of equations depends on the parameter values. The parameters of this system can be categorized into model parameters (C) and mean-flow deformation parameters.

https://doi.org/10.1017/S0022112000001336 Published online by Cambridge University Press

3. Equilibrium analysis

At the very least, the pressure–strain correlation model must produce the 'correct' equilibrium behaviour. The purpose of this section is to establish the causal relationship between the model's coefficients and its equilibrium behaviour. This can be accomplished by performing fixed point and bifurcation analyses of the anisotropy evolution equation. The structural equilibrium state of turbulence is described by the fixed points of the equations (17) and (18):

$$\frac{\mathrm{d}b_{ij}}{\mathrm{d}t} = 0 \quad \text{and} \quad \frac{\mathrm{d}\omega}{\mathrm{d}t} = 0. \tag{19}$$

At equilibrium, equations (17) and (18) indicate that the Reynolds stress is a tensor function of only the mean strain and rotation rates. Representation theory can then be invoked to determine the most general tensor function that can be constructed with the strain and rotation rates.

A brief introduction to representation theory based on the observations of Rubinstein (1999, private communication) is now provided. Representation theory has its roots in the classical invariant theory. The goal of representation theory is to exhibit an algebraically independent set of polynomial invariants, say of isotropic tensor functions of arbitrary order in a finite number of tensor variables, so that any polynomial invariant can be expressed in this basis. This has been accomplished for various special cases, the most relevant of which to the present work is the application of this theory to continuum mechanics by Rivlin (1957). Rivlin gives algebraic bases of isotropic functions of one-, two- and three-dimensional tensors.

In the present case, representation theory indicates that the most general physically permissible polynomial form for the Reynolds stress anisotropy in terms of the strain and rotation rates (for two-dimensional mean flow) is (Pope 1975; Girimaji 1996)

$$b_{ij} = G_1 S_{ij} + G_2(S_{ik}W_{kj} - W_{ik}S_{kj}) + G_3(S_{ik}S_{kj} - \tfrac{1}{3}\eta_1\delta_{ij}), \tag{20}$$

where

$$\eta_1 = S_{ij}S_{ij} \quad \text{and} \quad \eta_2 = W_{ij}W_{ij} \quad \text{so that} \quad \eta_1 + \eta_2 = 1. \tag{21}$$

In the above equations, G_1–G_3 are scalar functions of the invariants of strain and rotation rate tensors yet to be determined. During evolution of b_{ij}, G_1–G_3 will be functions of time as well.

The following identities are valid for all two-dimensional mean flows:

$$\left.\begin{aligned} S_{ik}S_{kj} &= \tfrac{1}{2}\eta_1\delta^{(2)}_{ij}, & W_{ik}W_{kj} &= -\tfrac{1}{2}\eta_2\delta^{(2)}_{ij}, \\ S_{ik}S_{kl}S_{lj} &= \tfrac{1}{2}\eta_1 S_{ij}, & S_{ik}W_{kl}S_{lj} &= -\tfrac{1}{2}\eta_1 W_{ij}, \\ W_{ik}S_{kl}W_{lj} &= \tfrac{1}{2}\eta_2 S_{ij}, & S_{mn}b_{mn} &= G_1\eta_1, \end{aligned}\right\} \tag{22}$$

where $\delta^{(2)}_{ij}$ and δ_{ij} are two- and three-dimensional Kronecker delta functions respectively. Using these rules, we write

$$\left.\begin{aligned} S_{ik}b_{kj} + b_{ik}S_{kj} - \tfrac{2}{3}b_{mn}S_{mn}\delta_{ij} &= \tfrac{1}{3}\eta_1 G_3 S_{ij} + 2G_1(S_{ik}S_{kj} - \tfrac{1}{3}\eta_1\delta_{ij}), \\ W_{ik}b_{kj} - b_{ik}W_{kj} &= -G_1(S_{ik}W_{kj} - W_{ik}S_{kj}) + 2\eta_2 G_2 S_{ij}. \end{aligned}\right\} \tag{23}$$

The anisotropy evolution equation can now be written in terms of its representation. Substitution of the anisotropy representation (equation (20)) into its evolution

https://doi.org/10.1017/S0022112000001336 Published online by Cambridge University Press

equation (17) followed by simplifications using equation (23) leads to

$$\begin{aligned}\frac{\mathrm{d}G_1}{\mathrm{d}t}S_{ij} + \frac{\mathrm{d}G_2}{\mathrm{d}t}(S_{ik}W_{kj} - W_{ik}S_{kj}) + \frac{\mathrm{d}G_3}{\mathrm{d}t}(S_{ik}S_{kj} - \tfrac{1}{3}\eta_1\delta_{ij}) \\ = -[G_1S_{ij} + G_2(S_{ik}W_{kj} - W_{ik}S_{kj}) + G_3(S_{ik}S_{kj} - \tfrac{1}{3}\eta_1\delta_{ij})](L_1^0\omega - L_1^1G_1\eta_1) \\ + L_2S_{ij} + L_3[\tfrac{1}{3}\eta_1G_3S_{ij} + 2G_1(S_{ik}S_{kj} - \tfrac{1}{3}\eta_1\delta_{ij})] \\ + L_4[-G_1(S_{ik}W_{kj} - W_{ik}S_{kj}) + 2\eta_2G_2S_{ij}]. \end{aligned} \tag{24}$$

The coefficients of each tensor on either side of the above equation have to be equal:

$$\left.\begin{aligned}\frac{\mathrm{d}G_1}{\mathrm{d}t} + G_1(L_1^0\omega - L_1^1G_1\eta_1) &= L_2 + \tfrac{1}{3}L_3G_3\eta_1 + 2L_4\eta_2G_2, \\ \frac{\mathrm{d}G_2}{\mathrm{d}t} + G_2(L_1^0\omega - L_1^1G_1\eta_1) &= -G_1L_4, \\ \frac{\mathrm{d}G_3}{\mathrm{d}t} + G_3(L_1^0\omega - L_1^1G_1\eta_1) &= 2G_1L_3.\end{aligned}\right\} \tag{25}$$

Equations (25) along with (18) constitute the nonlinear system of evolution equations for Reynolds stresses in homogeneous turbulence (with two-dimensional, time-invariant mean velocity gradients). Fixed point and bifurcation analyses of this system are now performed.

The equilibrium state description (19) can be restated as

$$\frac{\mathrm{d}G_1}{\mathrm{d}t} = \frac{\mathrm{d}G_2}{\mathrm{d}t} = \frac{\mathrm{d}G_3}{\mathrm{d}t} = \frac{\mathrm{d}\omega}{\mathrm{d}t} = 0. \tag{26}$$

Using the notation that the fixed point values are denoted by a superscript 0, the algebraic fixed point relations are (using $b_{mn}S_{mn} = G_1^0\eta_1$)

$$\left.\begin{aligned}2\omega^0(C_{e1} - 1)G_1^0\eta_1 + (C_{e2} - 1)(\omega^0)^2 &= 0, \\ -G_1^0(L_1^0\omega^0 - L_1^1G_1^0\eta_1) + L_2 + \tfrac{1}{3}L_3G_3^0\eta_1 + 2L_4\eta_2G_2^0 &= 0, \\ G_2^0(L_1^0\omega^0 - L_1^1G_1^0\eta_1) + G_1^0L_4 &= 0, \\ G_3^0(L_1^0\omega^0 - L_1^1G_1^0\eta_1) - 2G_1^0L_3 &= 0.\end{aligned}\right\} \tag{27}$$

This system of equations has five fixed points:

$$\omega^0 = 0, \quad G_1^0 = 0, \quad L_2 + \tfrac{1}{3}L_3G_3^0\eta_1 + 2L_4\eta_2G_2^0 = 0; \tag{28}$$

$$\omega^0 = 0, \quad G_1^0 = -\frac{1}{\sqrt{\eta_1}}Q_1, \quad G_2^0 = \frac{L_4}{L_1^1\eta_1}, \quad G_3^0 = -\frac{2L_3}{L_1^1\eta_1}; \tag{29}$$

$$\omega^0 = 0, \quad G_1^0 = +\frac{1}{\sqrt{\eta_1}}Q_1, \quad G_2^0 = \frac{L_4}{L_1^1\eta_1}, \quad G_3^0 = -\frac{2L_3}{L_1^1\eta_1}; \tag{30}$$

$$\omega^0 = -2\frac{C_{e1} - 1}{C_{e2} - 1}G_1^0\eta_1, \quad G_1^0 = -\frac{1}{\sqrt{\eta_1}}Q^*, \quad G_2^0 = \frac{L_4}{L^*\eta_1}, \quad G_3^0 = -\frac{2L_3}{L^*\eta_1}; \tag{31}$$

$$\omega^0 = -2\frac{C_{e1} - 1}{C_{e2} - 1}G_1^0\eta_1, \quad G_1^0 = +\frac{1}{\sqrt{\eta_1}}Q^*, \quad G_2^0 = \frac{L_4}{L^*\eta_1}, \quad G_3^0 = -\frac{2L_3}{L^*\eta_1}. \tag{32}$$

In the above equations, Q_1 and Q^* are defined as

$$Q_1 = \sqrt{-\frac{L_2}{L_1^1} + \frac{2}{3}\left(\frac{L_3}{L_1^1}\right)^2 - 2\left(\frac{L_4}{L_1^1}\right)^2\frac{1 - \eta_1}{\eta_1}}, \quad Q^* = \sqrt{-\frac{L_2}{L^*} + \frac{2}{3}\frac{L_3^2}{L^{*2}} - 2\frac{L_4^2}{L^{*2}}\frac{1 - \eta_1}{\eta_1}}, \tag{33}$$

https://doi.org/10.1017/S0022112000001336 Published online by Cambridge University Press

where

$$L^* = 2L_1^0 \frac{C_{e1} - 1}{C_{e2} - 1} + L_1^1. \tag{34}$$

In general flows, a negative value of G_1^0 is consistent with a gradient-diffusion-type effect. A positive value would imply counter-gradient diffusion. In the context of homogeneous flows, negative G_1 is associated with kinetic energy transfer from the mean to fluctuating field and positive G_1 indicates energy transfer in the opposite direction.

The quantity Q_1 is real only in the interval $\eta_1 \geqslant \eta_1^a$:

$$\eta_1 \geqslant \eta_1^a = \frac{2L_4^2}{-L_2 L_1^1 + \frac{2}{3}L_3^2 + 2L_4^2}. \tag{35}$$

Similarly, Q^* is real only when $\eta_1 \geqslant \eta_1^b$:

$$\eta_1 \geqslant \eta_1^b = \frac{2L_4^2}{-L_2 L^* + \frac{2}{3}L_3^2 + 2L_4^2}. \tag{36}$$

In the case of both SSG and LRR pressure–strain models $\eta_1^a > \eta_1^b$. The values η_1^a and η_1^b will soon be identified as the bifurcation points of the model system.

3.1. *Stability of fixed points*

In order to establish the stability of a fixed point, we need to determine if any small perturbation of the system away from the fixed point eventually returns to the fixed point after a sufficiently long time. This can be established most expeditiously by investigating the eigenvalues and eigenvectors of the Jacobian of the system linearized about the fixed point. Negative eigenvalues correspond to the attraction of the solution along the corresponding eigenvector. A positive eigenvalue repels the solution trajectory away from the fixed point along its eigenvector. For a fixed point to be stable all the eigenvalues must be negative, so that all trajectories in the neighbourhood of the fixed point are attracted towards the fixed point. If all permissible initial conditions are attracted to a fixed point, then it is globally asymptotically stable. The set of all initial conditions that ultimately evolve to a stable fixed point is called the basin of attraction of that fixed point. For a nonlinear set of equations, such as the one considered here, it is difficult to establish the basin of attraction or global stability and we will only seek to establish the local asymptotic stability of each of the fixed points. First, the various types of fixed points are listed.

1. Attractor: Real parts of all eigenvalues negative; stable fixed point.
2. Repeller: Real parts of all eigenvalues positive; unstable fixed point.
3. Saddle: Real parts of some eigenvalues positive and others negative; unstable fixed point.
4. Limit cycle: All eigenvalues purely imaginary; long-time solution is oscillatory.

The Jacobian of the equation system at any fixed point is given by

$$\mathbf{J} = \begin{pmatrix} -2(C_{e1}-1)G_1^0\eta_1 - 2\omega^0(C_{e2}-1) & -2\omega^0(C_{e1}-1)\eta_1 & 0 & 0 \\ -G_1^0 L_1^0 & -L_1^0\omega + 2G_1^0 L_1^1\eta_1 & 2L_4\eta_2 & \frac{1}{3}L_3\eta_1 \\ -G_2^0 L_1^0 & L_1^1\eta_1 G_2^0 - L_4 & -L_1^0\omega + L_1^1 G_1^0\eta_1 & 0 \\ -G_3^0 L_1^0 & L_1^1\eta_1 G_3^0 + 2L_3 & 0 & -L_1^0\omega + L_1^1 G_1^0\eta_1 \end{pmatrix}. \tag{37}$$

https://doi.org/10.1017/S0022112000001336 Published online by Cambridge University Press

Fixed point 1. This fixed point exists for the entire range of η_1 values and is given by

$$\omega^0 = 0, \quad G_1^0 = 0, \quad L_2 + \tfrac{1}{3}L_3 G_3^0 \eta_1 + 2L_4 \eta_2 G_2^0 = 0.$$

At this, and every other, fixed point G_2^0 and G_3^0 also satisfy (from equations (27)),

$$\frac{G_2^0}{G_3^0} = -\frac{L_4}{2L_3}, \tag{38}$$

leading to

$$G_2^0 = \frac{L_2 L_4}{\frac{2}{3}L_3^2\eta_1 - 2L_4^2\eta_2}, \quad G_3^0 = \frac{-2L_2 L_3}{\frac{2}{3}L_3^2\eta_1 - 2L_4^2\eta_2}. \tag{39}$$

The Jacobian at this fixed point is

$$\boldsymbol{J} = \begin{pmatrix} 0 & 0 & 0 & 0 \\ 0 & 0 & 2L_4(1-\eta_1) & \frac{1}{3}L_3\eta_1 \\ 0 & L_1^1\eta_1 G_2^0 - L_4 & 0 & 0 \\ 0 & L_1^1\eta_1 G_3^0 + 2L_3 & 0 & 0 \end{pmatrix}. \tag{40}$$

The eigenvalues of the Jacobian are

$$\lambda_1 = 0, \quad \lambda_2 = 0, \quad \lambda_3 = +\sqrt{\eta_1}L_1^1 Q^*, \quad \lambda_4 = -\sqrt{\eta_1}L_1^1 Q^*, \tag{41}$$

and the corresponding eigenvectors are

$$\left.\begin{aligned} \boldsymbol{v}_1 &= [1,0,0,0], \\ \boldsymbol{v}_2 &= \left[0,0,-\frac{L_3\eta_1}{6L_4(1-\eta_1)},1\right], \\ \boldsymbol{v}_3 &= [0,+\sqrt{\eta_1}L_1^1 Q^*, L_1^1\eta_1 G_2^0 - L_4, L_1^1\eta_1 G_3^0 + 2L_3], \\ \boldsymbol{v}_4 &= [0,-\sqrt{\eta_1}L_1^1 Q^*, L_1^1\eta_1 G_2^0 - L_4, L_1^1\eta_1 G_3^0 + 2L_3]. \end{aligned}\right\} \tag{42}$$

When Q^* is real ($\eta_1 \geqslant \eta_1^b$), λ_3 is positive and λ_4 is negative leading to this fixed point being a saddle and, hence, unstable. When $\eta_1 < \eta_1^b$ the fixed point is non-hyperbolic, that is, all eigenvalues of the linearized Jacobian have zero real parts. Linear analysis about the fixed point is inadequate to determine its stability. The more complicated centre manifold analysis needs to be performed to evaluate the stability characteristics. We will merely identify this fixed point as a limit cycle.

Fixed points 2 and 3. These fixed points are given by

$$\omega^0 = 0, \quad G_1^0 = \pm\frac{1}{\sqrt{\eta_1}}Q_1, \quad G_2^0 = \frac{L_4}{L_1^1\eta_1}, \quad G_3^0 = -\frac{2L_3}{L_1^1\eta_1}, \tag{43}$$

and exist only in the range $\eta_1 \geqslant \eta_1^a$.

The Jacobian of this fixed point is

$$\boldsymbol{J} = \begin{pmatrix} 0 & 0 & 0 & 0 \\ -G_1^0 & 2G_1^0\eta_1(L_1^1 + C_{e1} - 1) & 2L_4(1-\eta_1) & \frac{1}{3}L_3\eta_1 \\ -G_2^0 & 0 & G_1^0\eta_1(L_1^1 + 2C_{e1} - 2) & 0 \\ -G_3^0 & 0 & 0 & G_1^0\eta_1(L_1^1 + 2C_{e1} - 2) \end{pmatrix}. \tag{44}$$

The eigenvalues of fixed points 2 and 3 are given by

$$\lambda_1 = \mp 2(C_{e1} - 1)\sqrt{\eta_1}Q_1, \quad \lambda_2 = \pm 2L_1^1\sqrt{\eta_1}Q_1, \quad \lambda_3 = \lambda_4 = \pm L_1^1\sqrt{\eta_1}Q_1. \tag{45}$$

https://doi.org/10.1017/S0022112000001336 Published online by Cambridge University Press

The eigenvectors are

$$\left.\begin{aligned}
\boldsymbol{v}_1 &= \left[\frac{\eta_1}{L_1^0}(L_1^1 + 2C_{e1} - 2), \frac{G_1^0\eta_1(L_1^1 + 2C_{e2} - 2) + 2L_4\eta_2 + \frac{1}{3}L_3\eta_1}{2G_1^0\eta_1(L_1^1 + C_{e1} - 1)}, 1, 1\right], \\
\boldsymbol{v}_2 &= [0, 1, 0, 0], \\
\boldsymbol{v}_3 &= \left[0, -\frac{2L_4(1-\eta_1)}{G_1^0 L_1^1 \eta_1} 1, 0\right], \\
\boldsymbol{v}_4 &= \left[0, \frac{L_3}{3G_1^0 L_1^1} 0, 1\right].
\end{aligned}\right\} \tag{46}$$

For all of the models considered, L_1^1 and $(C_{e1} - 1)$ are both positive and η_1 is also positive by definition. As a result, some of the eigenvalues will be positive and others negative. Therefore, fixed points 2 and 3 are of the saddle type. These two fixed points are unstable when $\eta_1 > \eta_1^a$ and do not exist otherwise. They do not play an important role in the long-time behaviour of the Reynolds stress anisotropy.

If, however, the model coefficient C_{e1} is less than unity and L_1^1 is positive, all the eigenvalues of fixed point 2 will be positive and it will be a repeller. Fixed point 3 will then be an attractor since all its eigenvalues will be negative.

Fixed point 4. This fixed point is given by

$$\omega^0 = -2\frac{C_{e1} - 1}{C_{e2} - 1} G_1^0 \eta_1, \quad G_1^0 = -\frac{1}{\sqrt{\eta_1}} Q^*, \quad G_2^0 = \frac{L_4}{L^* \eta_1}, \quad G_3^0 = -\frac{2L_3}{L^* \eta_1}. \tag{47}$$

This fixed point exists only for $\eta_1 \geqslant \eta_1^b$ (see equation (36) for definition).

The Jacobian in this case cannot be simplified any further than that given in equation (37). Due to the complex nature of the Jacobian, it is difficult to obtain all the eigenvalues and eigenvectors symbolically. However, one eigenvalue is easily obtained by inspection:

$$\lambda_1 = G_1^0 \eta_1 L^*, \tag{48}$$

and the corresponding eigenvector is

$$\boldsymbol{v}_1 = \left[0, 0, 1, -6\frac{L_4(1-\eta_1)}{L_3\eta_1}\right]. \tag{49}$$

The eigenvalues are evaluated numerically and plotted in figure 1 as a function of the parameter η_1 for the linearized SSG pressure–strain correlation model. All of the eigenvalues are negative for all values of η_1, indicating that this is, indeed, an attracting fixed point. (Note that the quantity plotted is the negative of the actual eigenvalues.) Another important point to be gleaned from the figure is that eigenvalue λ_4 is always about an order of magnitude smaller than the other eigenvalues. This indicates that the solution evolves slowly along the eigenvector associated with λ_4 and rapidly along all other directions. The eigenvector direction corresponding to λ_4 is also shown in figure 1. This eigenvector is almost coincident with the ω-axis, indicating that ω evolves more slowly than the other three variables. All eigenvalues of this fixed point with the LRR pressure–strain correlation model (not shown) are also negative indicating an attracting fixed point. The LRR model eigenvalues are qualitatively similar to those of the SSG model.

https://doi.org/10.1017/S0022112000001336 Published online by Cambridge University Press

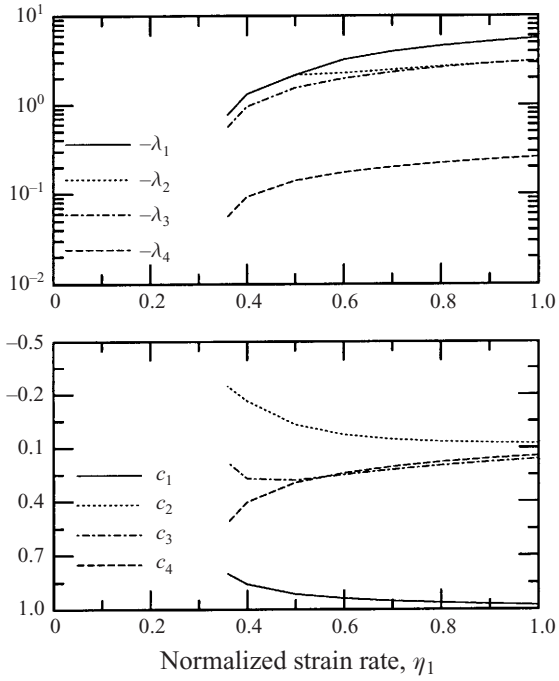


FIGURE 1. (*a*) Eigenvalues of fixed point 4 as a function of η_1. (*b*) Components of eigenvector corresponding to eigenvalue λ_4.

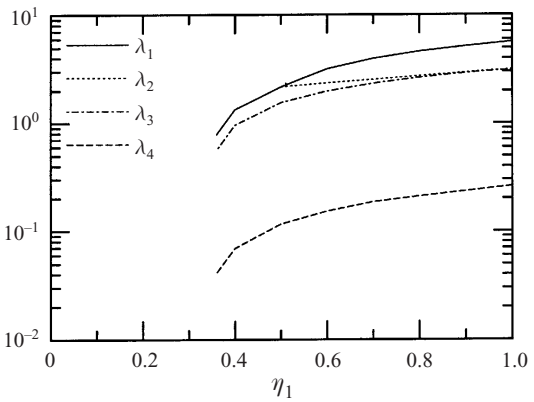


FIGURE 2. Eigenvalues of fixed point 5 as a function of η_1.

Fixed point 5. This fixed point

$$\omega^0 = -2\frac{C_{e1}-1}{C_{e2}-1}G_1^0\eta_1, \quad G_1^0 = +\frac{1}{\sqrt{\eta_1}}Q^*, \quad G_2^0 = \frac{L_4}{L^*\eta_1}, \quad G_3^0 = -\frac{2L_3}{L^*\eta_1}, \qquad (50)$$

also exists only for $\eta_1 \geqslant \eta_1^b$. The eigenvalues calculated numerically are shown in figure 2 for the SSG model. All of the eigenvalues are positive indicating that the fixed point is a repeller and, hence, unstable.

https://doi.org/10.1017/S0022112000001336 Published online by Cambridge University Press

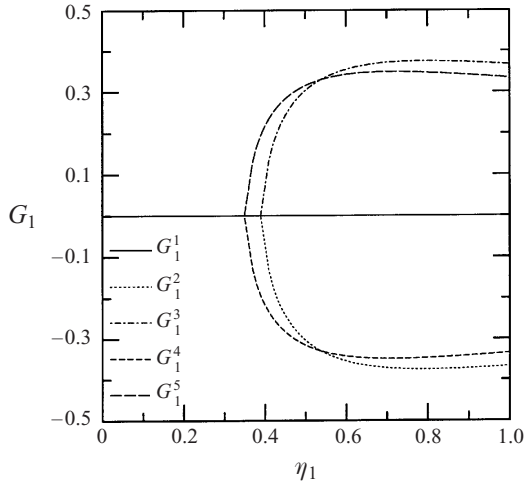


FIGURE 3. Bifurcation diagram of G_1^0 for SSG model. Fixed point G_1^1: unstable (saddle) for $\eta \geqslant \eta_1^b$ and centre for $\eta < \eta_1^b$. G_2, G_3: unstable (saddle). G_4: stable (attractor). G_5: unstable (repeller).

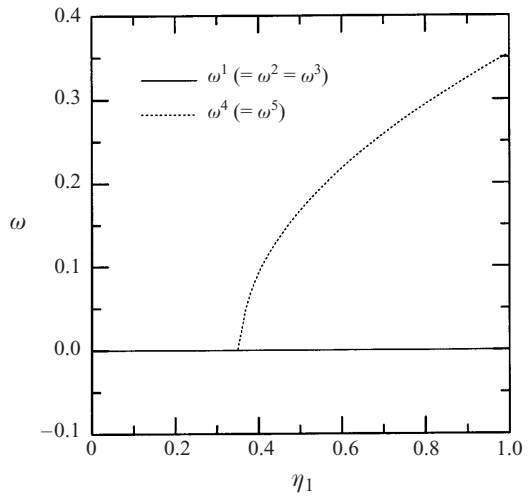


FIGURE 4. Bifurcation diagram of ω for SSG model. Fixed point $\omega^1 (= \omega^2 = \omega^3)$ is unstable (saddle) for $\eta \geqslant \eta 1_1^b$ and stable for $\eta < \eta_1^b$. $\omega^4 (= \omega^5)$ is stable (attractor).

3.2. *Bifurcation analysis*

For a given pressure–strain model, the equilibrium behaviour of the dynamical system of equations (17) and (18) depends solely upon the value of the deformation parameter η_1. The nature and even the number of fixed points of this system change with changing parameter values. The equation system has two bifurcation points, η_1^a and η_1^b. For the definitions of η_1^a and η_1^b, see equations (35) and (36).

In the interval $\eta_1 \in (\eta_1^a, 1)$, both Q_1 and Q^* are real, and all of the five fixed points exist. Of these, only 4 is stable (attractor). The system undergoes bifurcation at $\eta_1 = \eta_1^a$ when fixed points 2 and 3 cease to exist. In the interval $\eta_1 \in (\eta_1^b, \eta_1^a)$ only Q^* is real and the system has three fixed points (1, 4 and 5). Again, only fixed point 4 is attracting and others are unstable. The model system undergoes a second bifurcation at $\eta_1 = \eta_1^b$ when the attractor (point 4) and the repeller (point 5) vanish. Finally, in

https://doi.org/10.1017/S0022112000001336 Published online by Cambridge University Press

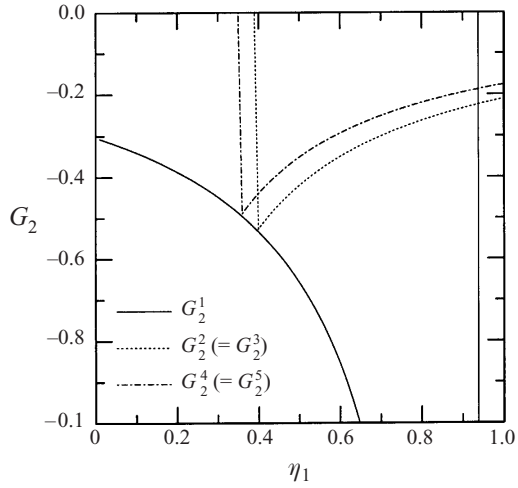


FIGURE 5. Bifurcation diagram of G_2^0 for SSG model.

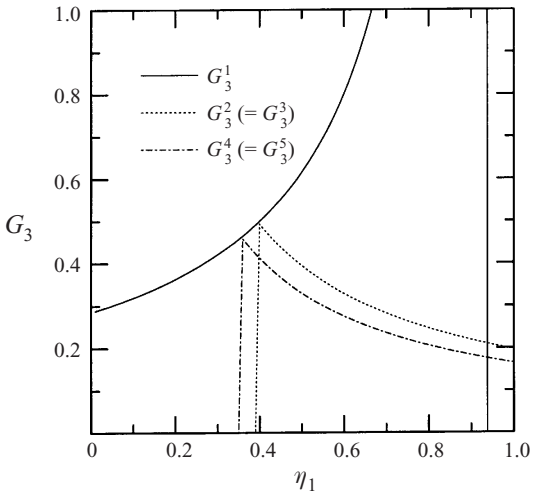


FIGURE 6. Bifurcation diagram of G_3^0 for SSG model.

the interval $\eta_1 \in (0, \eta_1^b)$, both Q_1 and Q^* are imaginary and the solution goes into a limit cycle about the only surviving fixed point, 1.

The bifurcation diagrams of G_1^0, ω^0, G_2^0 and G_3^0 as a function of the parameter η_1 are given in figures 3, 4, 5 and 6. The figures are shown for the SSG pressure–strain correlation model. The bifurcation diagram of G_1^0 for the LRR model is given in figure 7. The qualitative behaviour of the two models are nearly the same and only the bifurcation points are different: η_1^b is 0.25 for LRR and 0.35 for SSG.

Figures 5 and 6 reveal a possible flaw in the current models. It is seen that the equilibrium values G_2^0 and G_3^0 corresponding to fixed point 1 exhibit very large changes in the proximity of $\eta_1 = 0.8$. From equation (39), it is easily seen that the fixed point values become singular when

$$\eta_1(\text{singular}) = \frac{L_4^2}{L_4^2 + \frac{1}{3}L_3^2}. \tag{51}$$

https://doi.org/10.1017/S0022112000001336 Published online by Cambridge University Press

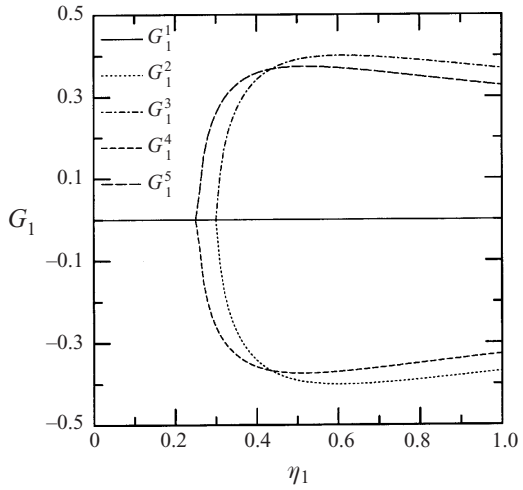


FIGURE 7. Bifurcation diagram of G_1^0 for LRR model. Fixed point G_1^1: unstable (saddle) for $\eta \geqslant \eta_1^b$ and centre for $\eta < \eta_1^b$. G_2, G_3: unstable (saddle). G_4: stable (attractor). G_5: unstable (repeller).

A model calculation with the initial condition in the vicinity of fixed point 1 with $\eta_1 \approx \eta_1$(singular) may exhibit abrupt and large changes in the values of anisotropy. Since there is no apparent sudden change in the physics of the Navier–Stokes equation at this parameter value, the model behaviour at this fixed point must be deemed unphysical. However, this flaw is not crucial since the equilibrium behaviour at this η_1 value is governed by fixed point 4 which is well behaved. The present modelling work does not address the rectification of this defect.

3.3. *Equilibrium behaviour of model system*

The fixed point and bifurcation analyses enable us to characterize the equilibrium behaviour of the model. The long-time behaviour of the model solution can be completely parameterized in terms of the deformation parameter η_1.

Long-time behaviour for $\eta_1 > \eta_1^b$. The system has multiple fixed points, but at long times all solution trajectories are attracted to fixed point 4. The anisotropy and timescale ratio converge monotonically to their respective non-zero fixed point values given in equation (47). The production to dissipation ratio at this equilibrium state is

$$\frac{P}{\varepsilon}(equilibrium) = \frac{C_{e2} - 1}{C_{e1} - 1} \tag{52}$$

for all η_1. In appropriately normalized time, the turbulent kinetic energy and dissipation grow exponentially:

$$\frac{\mathrm{d}\ln K}{\mathrm{d}\tau} = \frac{P}{\varepsilon} - 1, \quad \frac{\mathrm{d}\ln \varepsilon}{\mathrm{d}\tau} = C_{e1}\frac{P}{\varepsilon} - C_{e2}, \tag{53}$$

where $\tau = \omega_0 t$. If the equilibrium growth rates (in normalized time) are required to be functions of η_1, then the dissipation-equation model coefficients must have dependence on η_1.

Long-time behaviour for $\eta_1 < \eta_1^b$. In this parameter range, only one fixed point, 1, exists and it dictates the long-time behaviour of the solution. The solitary fixed point indicates that the character of the dynamical system is now linear. (Nonlinear systems are characterized by multiple fixed points.) In linear systems, the solution has

https://doi.org/10.1017/S0022112000001336 Published online by Cambridge University Press

a strong dependence on the initial conditions at all times. Therefore, the equilibrium behaviour of the system, in this parameter range, is very difficult to generalize. We present some features observed in numerical calculations:

1. ω decays monotonically to zero. Note that oscillation about zero is not permissible since a negative value of ω would violate realizability.

2. G_1 oscillates about zero. This is permitted. Negative values indicate positive production and positive values correspond to negative production.

3. G_2 and G_3 converge to non-zero values G_2^0 and G_3^0. While some components of the anisotropy tensor oscillate, the others go to their equilibrium values monotonically.

4. The production to dissipation ratio is no longer a constant and can be periodic depending upon the initial condition. The amplitude and frequency of the fluctuation depend upon η_1.

5. Very significantly, with decreasing η_1, the asymptotic growth rates of kinetic energy and dissipation decrease. For small enough η_1 values kinetic energy and dissipation decay in time leading to relaminarization.

The causal relationship between the model coefficients and its equilibrium behaviour is now listed:

C_1^0, C_1^1, C_2, C_3: Their most significant influence is on the equilibrium anisotropy (47). They play a secondary role in determining the bifurcation points of the system (35), (36).

C_4: This coefficient has the greatest influence in determining the bifurcation point. The closer the value of C_4 to 2, the smaller the η_1^b. The range of parameter values for which the turbulence is energetic increases as C_4 gets closer to 2. The LRR model ($C_4 = 1.31$) is energetic for a wider range of elliptic flows than the SSG model ($C_4 = 0.4$). This explains the marginally better predictions of LRR over SSG in elliptic flows observed by Blaisdell & Sharif (1996). This coefficient also influences equilibrium anisotropy values.

C_{e1}, C_{e2}: These two coefficients exclusively determine the growth rates of kinetic energy and dissipation (53). They also play a marginal role in determining the anisotropy and its bifurcation (34).

Three-dimensional and inhomogeneous flows. Fixed point analysis of homogeneous three-dimensional flows is very similar in concept, but its execution is rendered difficult by the large number of candidate tensors. Analysis of three-dimensional flows using a symbolic manipulator (MAPLE) is currently underway. Single-point fixed point analysis is, even conceptually, not possible for inhomogeneous flows. The presence of Reynolds stress gradients arising out of mean advection and turbulence transport terms complicates matters and a functional fixed point analysis is needed. In this case, rather than determining fixed point values, we will need to seek fixed point functions.

4. Equilibrium pressure–strain correlation model

In order to achieve the greatest degree of fidelity, the fixed point and bifurcation behaviour of the model must be matched with that of the physical (Navier–Stokes) system. However, the bifurcation behaviour of the physical system, especially that of the unstable fixed points, is difficult to determine. In this paper, we will only match the behaviour of those fixed points which determine the long-time solution.

In general, the pressure–strain correlation must be a function of the state of turbulence and the mean deformation. Any model coefficient (C_α) is, therefore, a scalar function of the invariants of the deformation and state of turbulence, equation (10).

https://doi.org/10.1017/S0022112000001336 Published online by Cambridge University Press

All the turbulence state variables at equilibrium are completely determined by mean flow deformation. The equilibrium coefficients are, therefore, functions exclusively of the mean deformation:

$$C_\alpha^{eq} = C_\alpha^{eq}(S_{ij}, W_{ij}). \tag{54}$$

The objective of this section is to determine C_α^{eq} by requiring that the bifurcation behaviour of the model system be consistent with that of the physical (Navier–Stokes) system. The model equilibrium behaviour was described in the previous section and that of the physical system needs to be established. We will restrict ourselves to the equilibrium behaviour of homogeneous two-dimensional mean flows of different strain to vorticity ratios. Vorticity-dominated elliptic flows are of particular interest since the current models appear to be satisfactory in strain-dominated flows.

4.1. *Equilibrium behaviour of physical system*

The equilibrium behaviour of elliptic streamline flows is inferred from the direct numerical simulation (DNS) and linear stability analysis results.

Blaisdell & Shariff (1996) have performed direct numerical simulations of several elliptic flows with different mean strain to rotation ratios. Initially, the mean-flow rotation suppresses the kinetic energy growth rate: the quicker the rotation, the larger and longer the suppression. At longer times, the nonlinearity is re-established as evidenced by the growth of turbulent kinetic energy and other statistics. They claim that for all ellipticity parameters, 'the turbulence seems to develop an asymptotic state that is independent of the ratio of mean rotation to mean strain'. The DNS data show no sign of bifurcation of equilibrium behaviour in the range of the ellipticity parameters considered.

The qualitative behaviour of elliptic flows can also be surmised from linear stability analysis (Speziale, Abid & Blaisdell 1996). Consistent with DNS observations, linear analysis indicates that all elliptic flows, even the most weakly strained ones, are energetic. It can be proven that flows that are linearly unstable will be unstable in nonlinear analysis also (Speziale *et al.* 1996). The pertinence of linear stability analysis results to Navier–Stokes physics is, therefore, very strong. Further, according to linear analysis, for a given strain rate, the higher the rotation rate, the higher is the kinetic energy growth rate. This feature is observed in DNS at intermediate times, before the nonlinear effects come into full play. These analytical results lend further credibility to the DNS results.

The equilibrium behaviour of the physical system, as inferred from DNS data and linear stability analysis, can be summarized as follows:

1. All elliptic flows are energetic at long times as the nonlinear effects prevail even in weakly strained cases. *There is no bifurcation in the long-time behaviour.*

2. The non-dimensional kinetic energy growth rate is independent of the strain to rotation rate ratio. This is true in all flows with non-zero strain rates.

3. The pure mean rotation (zero strain rate) flow represents a singular limit of elliptic flow behaviour. In this case, production is zero and the cascade is suppressed. Kinetic energy dissipates due to viscous action at all scales.

4.2. *Specification of model coefficients*

We will now specify model coefficients to capture important features of the equilibrium behaviour of the physical system summarized above. The model coefficients at equilibrium can be constant or functions of the invariants of deformation (equation (54)). The equilibrium values of the coefficients cannot be functions of the state of

https://doi.org/10.1017/S0022112000001336 Published online by Cambridge University Press

turbulence (b_{ij}, ω), for at equilibrium the mean deformation completely determines the state of turbulence. In two-dimensional mean flows, the only irreducible scalar invariants of the deformation tensor are η_1 and η_2. Since $\eta_1 + \eta_2 = 1$, there exists only one independent irreducible scalar invariant of the deformation tensor. We choose η_1, which is a ratio of strain to total deformation, as the independent invariant. Further, the bifurcation of the system depends upon the value of η_1. From the fixed point and bifurcation analysis, η_1 emerges as the natural choice of scalar function on which the equilibrium model coefficients must depend:

$$C_\alpha^{eq} = C_\alpha^{eq}(\eta_1). \tag{55}$$

We now seek to identify this functional dependence.

The most important feature of the long-time behaviour of the physical system is its bifurcation. If the bifurcation points of the model and physical systems do not coincide, the model will be, even qualitatively, wrong. It will be seen later that the bifurcation behaviour of the LRR and SSG models is quite different from that observed in the DNS. This results in the gross disagreement between models and data in elliptic flows. Here, we attempt to match the bifurcation points of the model and physical systems.

The results for the physical system lead to one incontrovertible inference: *there is no bifurcation of equilibrium behaviour of turbulent elliptic flows for finite strain rate.* The bifurcation occurs at $\eta_1^b = 0$, the pure rotation limit:

$$\eta_1^b = \frac{2L_4^2}{-L_2L^* + \frac{2}{3}L_3^2 + 2L_4^2} = 0, \tag{56}$$

leading to

$$L_4(\eta_1 = 0) = 0 \quad \Rightarrow \quad C_4^{eq}(\eta_1 = 0) = 2. \tag{57}$$

For non-zero values of L_4, the model long-time behaviour will bifurcate at finite values of η_1, contrary to observed physics.

The traditional value for C_4 is known to yield the right equilibrium behaviour for the strain-dominated flows ($\eta_1 > 0.5$). Based on these facts, we propose the following:

$$C_4^{eq} = \begin{cases} C_4^* & \text{for } \eta_1 \geqslant 0.5 \\ 2.0 - (2.0 - C_4^*) f_4(\eta_1) & \text{for } \eta_1 < 0.5. \end{cases} \tag{58}$$

In the above equation, C_4^* is the traditionally used value and $f_4(\eta_1)$ is a function which is to be determined.

Since the bifurcation must not occur at any value of η_1, the functional dependence of L_4 on η_1 should be such that (see equation (36))

$$\eta_1 > \frac{2L_4^2}{-L_2L^* + \frac{2}{3}L_3^2 + 2L_4^2}. \tag{59}$$

This requires that

$$\eta_1(-L_2L^* + \tfrac{2}{3}L_3^2) > 2L_4^2(1 - \eta_1) \quad \Rightarrow \quad L_4^2 < \frac{\eta_1}{2(1-\eta_1)}(-L_2L^* + \tfrac{2}{3}L_3^2), \tag{60}$$

leading to

$$L_4 < \sqrt{\frac{\eta_1}{1-\eta_1}}. \tag{61}$$

https://doi.org/10.1017/S0022112000001336 Published online by Cambridge University Press

This suggests the following form for f_4:

$$f_4 = \left(\frac{\eta_1}{1-\eta_1}\right)^n \quad \text{where } n > 0.5. \tag{62}$$

Good agreement with a variety of flows has been obtained with $n = 0.75$.

Other pressure–strain model coefficients. The values of the other coefficients of the pressure–strain correlation model do not play a crucial role in determining the bifurcation point, and, as a first step, will be treated as constants in this paper. In the future, we will specify these model coefficients as functions of the strain rate also by requiring closer fidelity with observed anisotropy values at the equilibrium state of turbulence. The detailed DNS data, for a variety of strain and rotation dominated flows, required for this purpose are not currently available.

Dissipation equation coefficients. The dissipation-equation model coefficients exclusively control the production to dissipation ratio and the growth rates of kinetic energy and dissipation in equilibrium turbulence (equation (53)). The DNS data indicate (inconclusively) that the non-dimensional growth rates are nearly independent of the strain–rotation ratio. Therefore, dissipation-equation model coefficients at the equilibrium state must also be independent of the strain–rotation ratio as in the current model. It is, therefore, well justified to leave the dissipation model equation (equilibrium) coefficients unchanged at their traditional constant values.

5. Non-equilibrium modelling

The rapid distortion limit, in which the imposed mean deformation rate is much larger than the turbulence deformation rate, represents the extreme state of non-equilibrium turbulence. It is generally recognized that the turbulence behaves like a viscous fluid in the equilibrium state ($\omega \sim 1$) and an elastic fluid in the rapid distortion state ($\omega \ll 1$), Crow (1968). In the equilibrium state, the turbulent stresses are dependent on the imposed deformation rate, whereas in the rapid distortion limit, they are dependent on the total deformation. This clearly indicates the need for developing separate pressure–strain correlation models for these two states of turbulence. In any intermediate (moderately non-equilibrium) state, the turbulence will exhibit a combination of viscous and elastic properties. If the turbulence physics is regular between the two extreme states, the model for intermediate states can be determined by suitably interpolating between the two limiting behaviours. A pressure–strain model in the rapid distortion limit is now sought.

When the Navier–Stokes equations for the fluctuating velocity field are considered in the rapid distortion limit, the terms nonlinear in fluctuations can be neglected. The resulting linear equations form the basis of the rapid distortion theory (RDT). Due to their linearity, the RDT equations are closed, but only at the two-point level. The lack of closure at the one-point level is due to the non-locality of the pressure field. Since we are interested in a one-point closure for the pressure–strain model, much of the RDT results cannot be used without further simplifying assumptions. Kassinos & Reynolds (1994) have developed sophisticated one-point closures for the pressure–strain correlations in the RDT limit that involve knowledge of two additional tensors. For the sake of simplicity, we will restrict ourselves to the more elementary RDT result of Crow (1968). The implementation of the Kassinos & Reynolds (1994) model into the current methodology is deferred to a later time.

When isotropic turbulence is subjected to a large shear, the Reynolds stresses

https://doi.org/10.1017/S0022112000001336 Published online by Cambridge University Press

evolve, to leading order, according to (Crow 1968)

$$b_{ij} \approx -\tfrac{2}{15} t S_{ij} \quad \text{for} \quad t \to 0. \tag{63}$$

The pressure–strain correlation consistent with the above evolution is

$$\phi_{ij} = \tfrac{4}{5} K S_{ij} \quad \Rightarrow \quad C_2^{rd} = \tfrac{4}{5}. \tag{64}$$

This is the value of C_2 in many of the constant-coefficient pressure–strain correlation models including LRR. While this value is appropriate in the rapid distortion limit, Speziale *et al.* (1991) find that a value of $C_2^{eq} = 0.36$ is better suited for the equilibrium state.

Other model coefficients. Given our limited current knowledge, it is not very clear what the other model coefficients (including dissipation model coefficients) must be in the rapid distortion limit. The currently used model coefficients (numerical constants) have been calibrated well in a large variety of important flows. There is no compelling reason to modify them at the rapid distortion state. These coefficients will be left unchanged at their equilibrium values until RDT can furnish their values more precisely. Again, as more results emerge, these coefficients should be modified accordingly.

5.1. *Interpolation for intermediate states*

The intermediate non-equilibrium state of turbulence is difficult to analyse as all of the different physical processes play important roles and the governing equations have to be considered in their full complexity. Mere quantification of the intermediate stage, even at a phenomenological level, has not been attempted previously. In this paper, we adopt a more pragmatic approach. Knowing the model coefficient values in the two extreme states, we propose to obtain the coefficients in the intermediate states by matched asymptotic expansion or any other formal procedure. Even if such a formal approach is possible, it is likely to be quite complicated and we propose a simple interpolation that yields desired results in test cases. The choice of the turbulence-state interpolation parameter can be made with more mathematical rigour. Clearly, the interpolation parameter must be a scalar function involving state variables of turbulence $-b_{ij}$ and ω. Exclusive dependence of the interpolation parameter on the mean strain and rotation invariants is deemed unphysical, for they contain no indication of the turbulence state. The scalar invariants that are suitable for interpolation are $-\omega$, $b_{ij}b_{ji}$, $b_{ij}b_{jk}b_{ki}$, $b_{ij}S_{ij}$, $b_{ij}S_{jk}S_{ki}$ and $b_{ij}S_{jk}W_{ki}$.

For the sake of simplicity, we choose only the timescale ratio (ω) to indicate the state of turbulence and serve as the interpolation parameter. The rapid distortion limit is characterized by $\omega \to 0$ and the equilibrium state by $\omega \to \omega^0$. The equilibrium strain rate, ω^0, is completely determined by the applied mean deformation and the equilibrium values of the model coefficients. For the intermediate states, we propose

$$C_2 = C_2(\omega). \tag{65}$$

The best agreement with data, in the test cases considered, is given by

$$C_2 = C_2^{rd} - (C_2^{rd} - C_2^{eq})\,[\omega/\omega^0]^{0.25}. \tag{66}$$

6. Results and discussion

The results obtained from the new model are compared to available DNS, LES and RDT data in elliptic flows, rotating shear flows and rapidly distorted turbulence.

https://doi.org/10.1017/S0022112000001336 Published online by Cambridge University Press

Results from computations using the SSG pressure–strain model is also provided for comparison. The new model used in the computations is now summarized:

$$\phi_{ij} = -(C_1^0\varepsilon + C_1^1 P)b_{ij} + C_2 K S_{ij} + C_3 K(b_{ik}S_{jk} + b_{jk}S_{ik} - \tfrac{2}{3}b_{mn}S_{mn}\delta_{ij}) + C_4 K(b_{ik}W_{jk} + b_{jk}W_{ik})$$

where

$$\left.\begin{aligned} & C_1^0 = 3.4,\ C_1^1 = 1.8,\ C_2^* = 0.36,\ C_3 = 1.25,\ C_4^* = 0.4; \\ & C_{e1} = 1.44,\ C_{e2} = 1.88; \\ & C_2 = \begin{cases} C_2^* & \text{for } \omega/\omega^0 \geqslant 1 \\ 0.8 - (0.8 - C_2^*)(\omega/\omega^0)^{0.25} & \text{for } \omega/\omega^0 < 1; \end{cases} \\ & C_4 = \begin{cases} C_4^* & \text{for } \eta_1 \geqslant 0.5 \\ 2.0 - (2.0 - C_4^*)[\eta_1/(1-\eta_1)]^{0.75} & \text{for } \eta_1 < 0.5. \end{cases} \end{aligned}\right\} \tag{67}$$

Choice of model coefficients. As seen in the previous sections, the choice of the new model coefficients is guided by bifurcation analysis and rapid distortion theory. Modifications to the coefficients beyond what is suggested by the above two methodologies is kept to a minimum. Further, the model coefficients that are not addressed in the two analyses are left unmodified at their standard constant values pending further investigations. Although the agreement of the model with data in the test cases considered can be further improved by *ad hoc* changes, it is not attempted here. The purpose of this article is to demonstrate that a few rational modifications can substantially improve the predictive capability of the standard form of the pressure–strain correlation model in flows previously considered unamenable to this class of models.

Elliptic flows. It is now well documented that the LRR and SSG pressure–strain correlation models perform very poorly in elliptic streamline flows (Blaisdell & Sharif 1996). Blaisdell & Sharif (1996) consider homogeneous turbulence subjected to the following mean flow:

$$\frac{\partial U_i}{\partial x_j} = \begin{pmatrix} 0 & 0 & -\gamma - e \\ 0 & 0 & 0 \\ \gamma - e & 0 & 0 \end{pmatrix}, \tag{68}$$

where $e = \sqrt{\eta_1/2}$ and $\gamma = \sqrt{(1-\eta_1)/2}$. When $0 < |e| < |\gamma|$, the mean streamlines are elliptic with an aspect ratio of $E \equiv \sqrt{(\gamma + e)(\gamma - e)}$. The data used here come from three simulations with ellipticity aspect ratios of 1.5, 2.0 and 3.0. These correspond to η_1 (ratio of strain to total deformation) values of approximately 0.13, 0.26 and 0.39. The turbulence field is initially isotropic and the initial mean-flow to turbulence timescale ratio for all three cases is $\varepsilon_0/SK_0 = 0.167$. The initial values for the kinetic energy and dissipation were taken from the DNS data: $K_0 = 0.0428$ ($E = 1.5$), 0.04566 ($E = 2.0$), 0.04857 ($E = 3.0$); $\varepsilon_0 = 0.12767$ ($E = 1.5$), 0.14531 ($E = 2.0$), 0.16443 ($E = 3.0$).

The kinetic energy evolution calculated from DNS is compared to the Reynolds stress closure model (RSCM) predictions in figure 8. As demonstrated in previous studies, the SSG model does poorly. For the $\eta_1 = 0.13$ and $\eta_1 = 0.26$ cases, the model predicts kinetic energy decay while the DNS data show vigorous growth. For the $\eta_1 = 0.39$ case, which has a larger component of strain, the SSG model does predict

https://doi.org/10.1017/S0022112000001336 Published online by Cambridge University Press

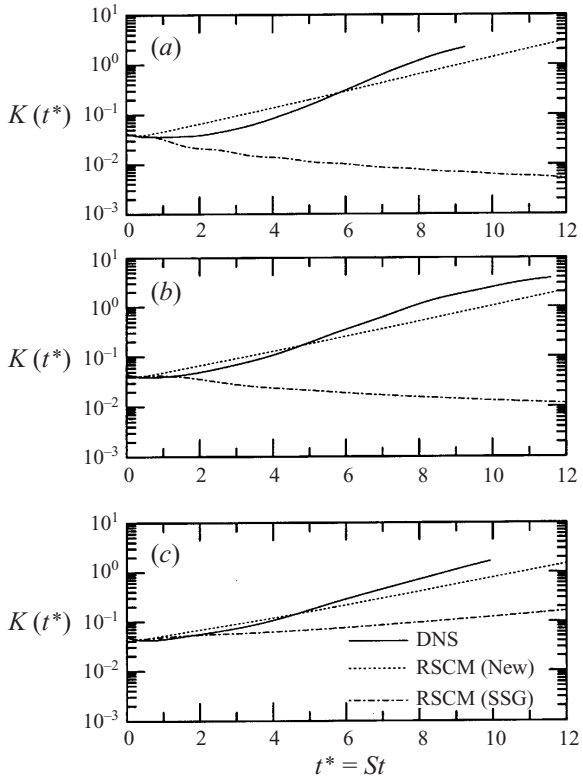


FIGURE 8. Evolution of kinetic energy in elliptic flows. DNS data from Blaisdell & Sharif (1996). (*a–c*) correspond to ellipticity factors of 1.5, 2.0 and 3.0. These correspond to $\eta_1 = 0.13, 0.26$ and 0.39.

kinetic energy growth, but at a rate much smaller than the observed rate. The present model captures the kinetic energy growth quite well for all aspect ratios considered, especially at later times.

The predicted turbulent shear stress anisotropy, b_{13}, is compared with DNS data in figure 9. This component of anisotropy determines the production and is crucial for correct prediction of the kinetic energy evolution. As can be seen, the present model captures the equilibrium behaviour of the anisotropy very well. The SSG model on the other hand, is quite wrong. For $\eta_1 = 0.13$ and $\eta_1 = 0.26$ it predicts an equilibrium value of nearly zero compared to the DNS value of nearly 0.2.

The comparison of the dissipation rate is shown in figure 10. Consistent with previous results, the present model performs well for all cases and the SSG model calculations are, even qualitatively, wrong. The normal anisotropy components b_{11} and b_{33} are compared in figures 11 and 12, respectively. Neither model performs particularly well. The SSG model appears to capture the initial transition behaviour a little better than the new model. But closer to the equilibrium state, the present model performs better.

On the whole, the present model captures the evolution of kinetic energy, dissipation and shear stress anisotropy extremely well. The normal anisotropy components evolution is not as well simulated, although the equilibrium values are reproduced adequately.

The poor performance of the SSG is easily understood in the context of the fixed

https://doi.org/10.1017/S0022112000001336 Published online by Cambridge University Press

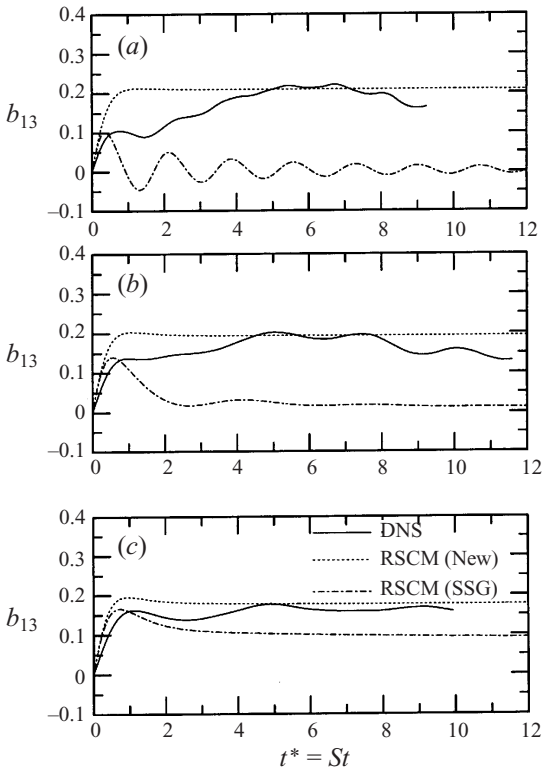


FIGURE 9. Evolution of b_{13} energy in elliptic flows. DNS data from Blaisdell & Sharif (1996).

point analysis performed in § 3. The long-time solution of the SSG model bifurcates at $\eta_1^b \approx 0.35$ (see figure 3). The physical system shows no bifurcation for finite values of η_1. Therefore, the SSG solution for $\eta_1 < 0.35$ will be even qualitatively wrong. This is readily seen in the comparisons of the $\eta_1 = 0.13$ and $\eta_1 = 0.26$ cases: the behaviour of the physical system (DNS) and model system is completely different. As indicated by the bifurcation diagram (figure 3), the model system predicts zero value for turbulent shear stress in these cases. The model predictions are qualitatively correct when $\eta_1 = 0.39$, in which case the fixed point is an attractor, rather than a limit cycle. The LRR model can be expected to perform a little better (than the SSG model) since its bifurcation value $\eta_1^b \approx 0.25$ is closer to the observed value of zero. Blaisdell & Sharif (1996) do, in fact, find this to be the case.

Bifurcation, or lack thereof, is also responsible for another feature seen in the model calculations of anisotropy. In low-η_1 calculations, the SSG model predicts oscillatory behaviour (also seen in DNS data) whereas the present model does not. The explanation is very simple. Due to lack of bifurcation, the long-time behaviour of the present model is always determined by the attracting fixed point 4. The fixed-coefficient models, however, undergo bifurcation and their long-time behaviour is determined by the limit-cycle fixed point 1. While the new model does kill the oscillatory behaviour, this is off-set by the fact that it converges to the correct equilibrium value. The other models oscillate about completely wrong values. Of course, it would be preferable for the model to oscillate about the right value. For this we would need fixed point 4 to be a spiral attractor (eigenvalues with negative real

https://doi.org/10.1017/S0022112000001336 Published online by Cambridge University Press

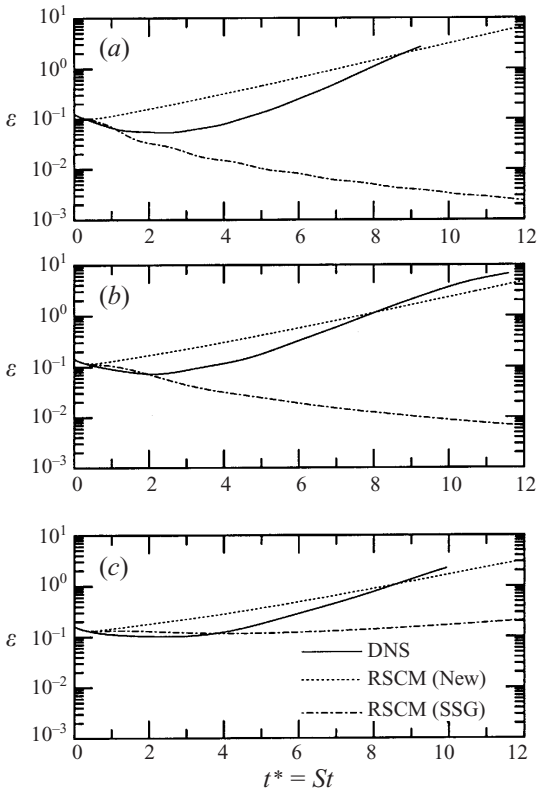


FIGURE 10. Evolution of dissipation in elliptic flows. DNS data from Blaisdell & Sharif (1996).

part and non-zero imaginary parts) rather than a focus-type attractor (zero imaginary parts). Major revamping of the pressure–strain correlation model form would be necessary to accomplish this change and is not attempted here.

There is some ambiguity regarding the precise DNS values of the anisotropy components at equilibrium. There is a potential danger of calibrating the model coefficients to inconclusive or incorrect DNS calculations. However, one conclusion from the DNS data is unequivocal. All elliptic flows are energetic in the equilibrium state, an observation that is corroborated by linear analysis. The limiting value of coefficient $C_4(= 2)$ is chosen to be consistent with this observation. Just this modification is quite adequate to give reasonable prediction of the anisotropy components, validating our methodology. When the anisotropy equilibrium values are known with more certainty, the other coefficients will be modified to yield better agreement.

Rotating flows. Turbulent flows subject to reference-frame rotation and mean-flow rotation share many similarities. Yet these two forms of rotation have contrasting effects on the fluctuating velocity field. The LRR and SSG models are better suited for frame-rotation flows: in fact the SSG model is calibrated in rotating shear flows. With these models, the correct behaviour in rotating flows precludes good performance in elliptic flows. This raises the important question of whether the present model, which performs well in elliptic flows, is capable of predicting rotating flows.

We compare the results of the present model and the SSG model to the rotating shear flow large-eddy simulation (LES) data of Bardina, Ferziger & Reynolds (1983). The reference-frame rotation rate is given by Ω and the velocity gradient in the

https://doi.org/10.1017/S0022112000001336 Published online by Cambridge University Press

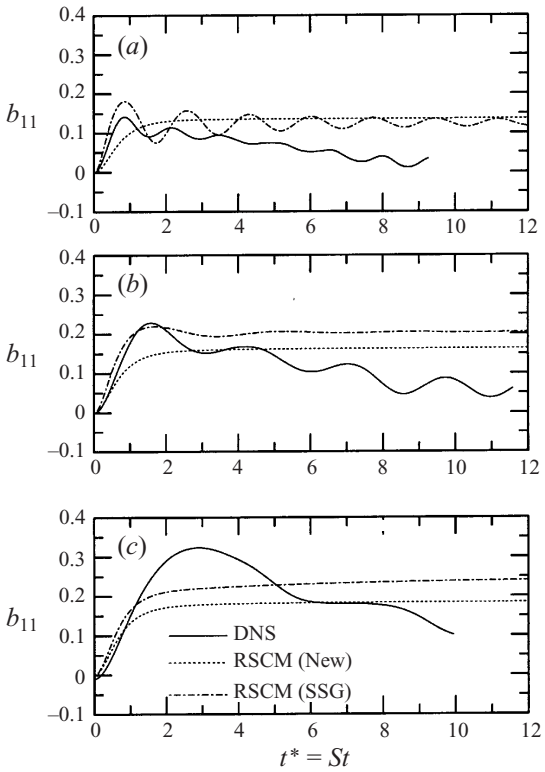


FIGURE 11. Evolution of b_{11} in elliptic flows. DNS data from Blaisdell & Sharif (1996).

rotating frame by

$$\frac{\partial U_i}{\partial x_j} = \begin{pmatrix} 0 & S & 0 \\ 0 & 0 & 0 \\ 0 & 0 & 0 \end{pmatrix}. \tag{69}$$

The turbulence field is initially isotropic. Three cases of the non-dimensional rotation rate, $\Omega/S = 0.25, 0.5, -0.5$ are considered. The initial mean-flow to turbulence timescale ratio for all three cases is $\varepsilon_0/SK_0 = 0.296$.

The strain and rotation rate tensors corresponding this flow are

$$S_{ij} = \tfrac{1}{2}S \begin{pmatrix} 0 & 1 & 0 \\ 1 & 0 & 0 \\ 0 & 0 & 0 \end{pmatrix}, \quad W_{ij} = \tfrac{1}{2}S\left(1 - 2\frac{\Omega}{S}\right) \begin{pmatrix} 0 & 1 & 0 \\ -1 & 0 & 0 \\ 0 & 0 & 0 \end{pmatrix}. \tag{70}$$

For determining the modification to C_4 we need

$$\frac{\eta_1}{1-\eta_1} = \frac{1}{(1-2\Omega/S)^2}. \tag{71}$$

The comparison of the kinetic energy evolution is given in figure 13(*a*) for $\Omega/S = 0.25$. Similar comparisons for the other two cases are given in figures 13(*b*) and 13(*c*). The SSG and the present model results are indistinguishable as they both predict the data well. In fact, in the decaying case, the present model appears to be somewhat better than the SSG model. The K–ε model calculations are insensitive to rotation and, hence, cannot capture the stabilizing effects of frame rotation.

https://doi.org/10.1017/S0022112000001336 Published online by Cambridge University Press

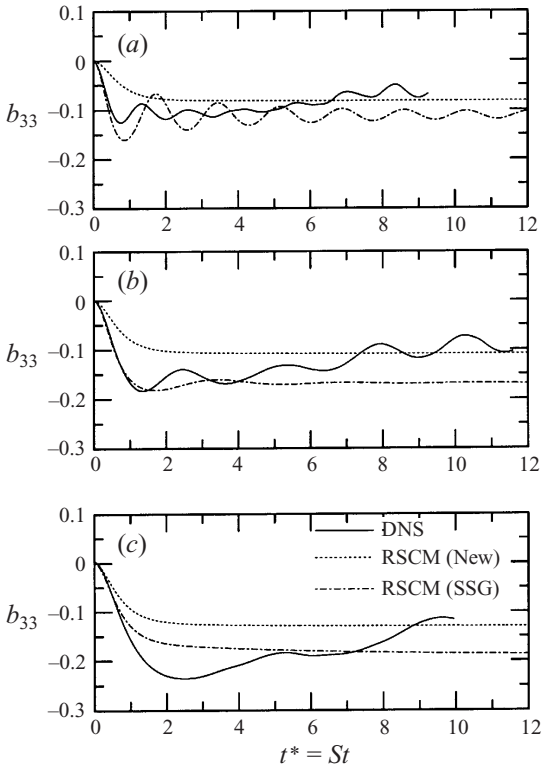


FIGURE 12. Evolution of b_{33} in elliptic flows. DNS data from Blaisdell & Sharif (1996).

Rapidly distorted flows. Rapidly distorted homogeneous shear and plane strain flows are considered. In the homogeneous shear flow case, the models are compared to the RDT solution for the case of $SK_0/\varepsilon_0 = 100$. The RDT solution is a good approximation for DNS at early times, in this case for up to $St = 10$. The kinetic energy growth rates are shown in figure 14. The SSG model, which is formally valid only near equilibrium, overpredicts the growth rate of the turbulent kinetic energy. This is due to the fact that the near-equilibrium models exaggerate the role of nonlinear effects in the rapid distortion limit. The new model, which is consistent with linear theory (Crow constraint) at this limit, produces excellent agreement.

Next, the comparison is performed in a rapidly distorted plane strain case: $\Gamma K_0/\varepsilon_0 = 100$. The data at early times ($t^* < \Gamma t$) come from the DNS of Lee & Reynolds (1985) and at later times from an RDT solution. The evolution of turbulent kinetic energy is given in figure 15. Again the performance of the present model is good and the SSG model is also quite adequate.

On the whole, the new model captures the evolution of kinetic energy very well in rapidly distorted flows. Given its good performance in the two extreme limits of turbulence, the rapid distortion and equilibrium states, one can be optimistic about its performance in general non-equilibrium flows.

6.1. *Inhomogeneous turbulent flows*

The objective of this and most other turbulence modelling efforts is to develop models suitable for computing complex flows of practical interest. Nearly all flows of engineering interest are inhomogeneous. While homogeneous turbulence serves as

https://doi.org/10.1017/S0022112000001336 Published online by Cambridge University Press

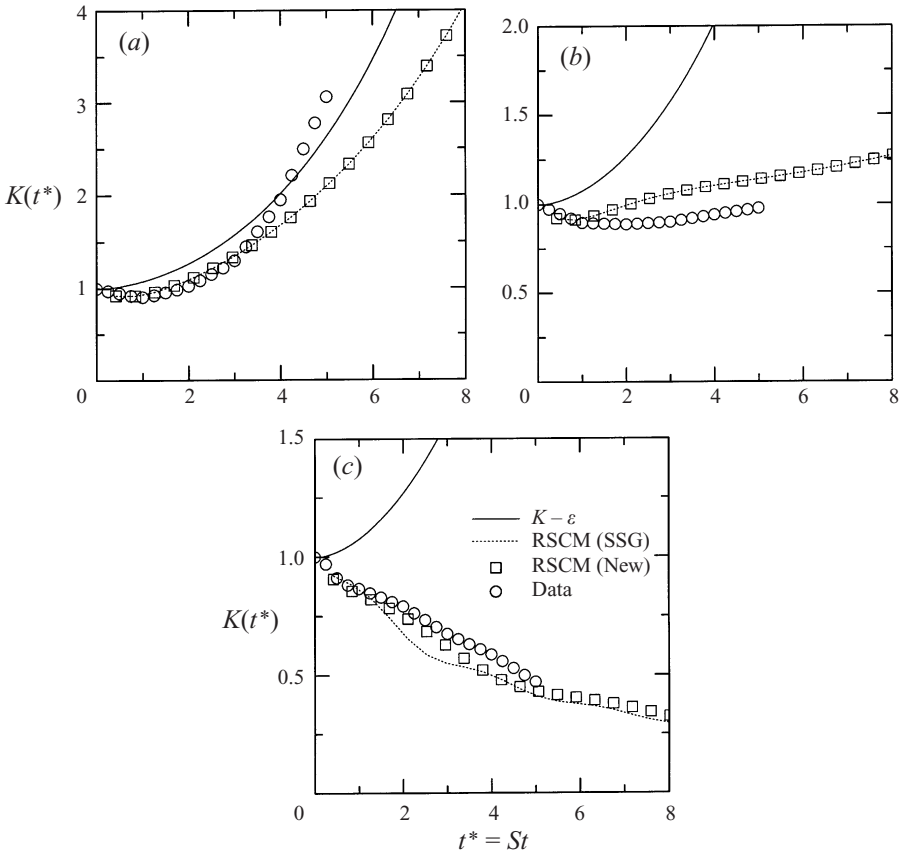


FIGURE 13. Evolution of kinetic energy in rotating flow with (*a*) $\Omega/S = 0.25$, (*b*) 0.50, (*c*) -0.50; $K_0 = \varepsilon_0 = 1$. LES data from Bardina *et al.* (1983).

an important test bed for developing and testing models, pressure–strain correlation models must ultimately be judged by their performance in inhomogeneous flows. Yet, there are some models that perform poorly in homogeneous turbulence but, remarkably, well in some inhomogeneous flows. This good performance in complex flows (while failing in simple ones) is usually attributable to cancellation of errors, rather than any inherent merit of the model. So it is important that a turbulence model perform well in simple as well as complex flows. We have already established that the new model performs very well in homogeneous turbulence. To be a useful tool for computing complex inhomogeneous flows, a pressure–strain correlation model must possess three important attributes: (i) accuracy; (ii) robustness; and (iii) computational viability. The present model has the traditional form and requires no more computational effort than the standard pressure–strain models. Robustness is a very important feature. Often in practice, a robust model of limited accuracy is preferred over an accurate less robust model. For inhomogeneous flows, Thangam, Wang & Girimaji (1998) point out that the present model is more robust than the SSG model. When both the models are integrated to the wall, the present model needs no modifications whereas the SSG model requires the inclusion of (somewhat arbitrary) damping functions. This is an important virtue for calculating internal bounded flows. Now we will evaluate the accuracy of the present model in two inhomogeneous flows.

https://doi.org/10.1017/S0022112000001336 Published online by Cambridge University Press

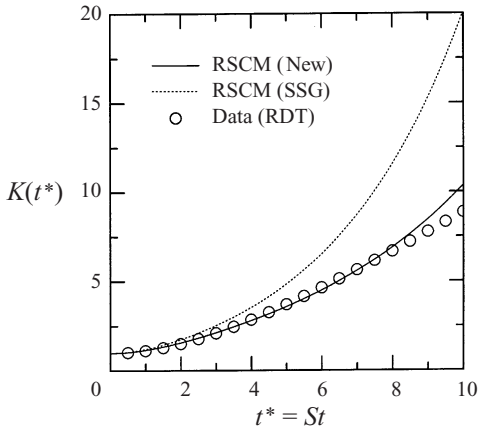


FIGURE 14. Evolution of kinetic energy in rapidly distorted homogeneous shear flow. $SK_0/\varepsilon_0 = 100$, $K_0 = \varepsilon_0 = 1$. Data from RDT calculations.

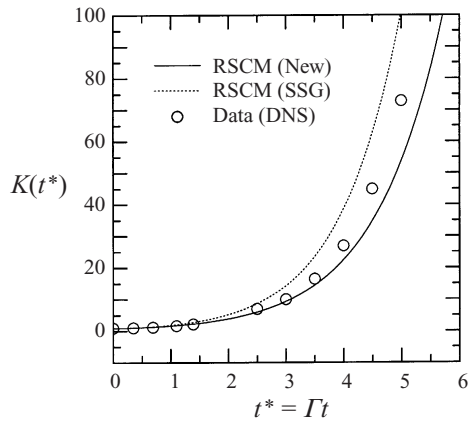


FIGURE 15. Evolution of kinetic energy in rapidly distorted plane strain flow. $\Gamma K_0/\varepsilon_0 = 100$, $K_0 = \varepsilon_0 = 1$. First five data points from DNS of Lee & Reynolds (1985). Remainder from RDT calculations.

Rotating channel flow. A complex inhomogeneous turbulent flow that is becoming an important benchmark for assessing pressure–strain correlation models is the rotating channel flow. This flow incorporates several flow features that the early pressure–strain correlation models do not reproduce accurately. Thangam *et al.* (1998) calculate the rotating channel flow using the new model and present detailed results. One sample result is shown here. The mean flow in a rotating channel calculated using the new pressure–strain correlation model is shown in figure 16. The asymmetry in the mean flow is well captured by the new model. The turbulent Reynolds stresses are well reproduced (figures not shown).

Trailing vortex calculations. Far from being of academic interest only, elliptic streamline flows appear in some important practical applications. The lifting surfaces (wings) of an aircraft generate two counter-rotating vortices in its wake. An encounter between these vortices and any trailing aircraft can be quite hazardous and therefore detailed knowledge of the vortex behaviour is very important. The evolution of these trailing vortices in an ambient straining field is quite similar to elliptic streamline

https://doi.org/10.1017/S0022112000001336 Published online by Cambridge University Press

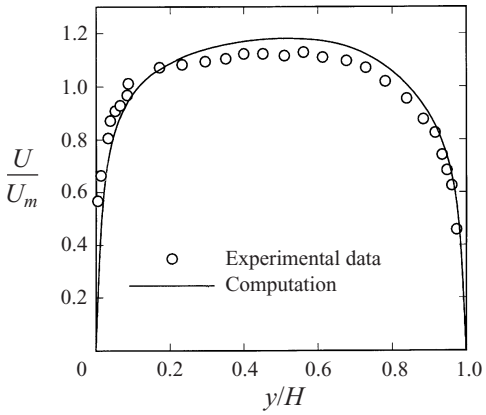


FIGURE 16. Mean velocity profile in a rotating channel ($Re = 11\,500; Ro = 0.069$). ○, Experiments by Johnston, Halleen & Lezius (1972); ——, present computations.

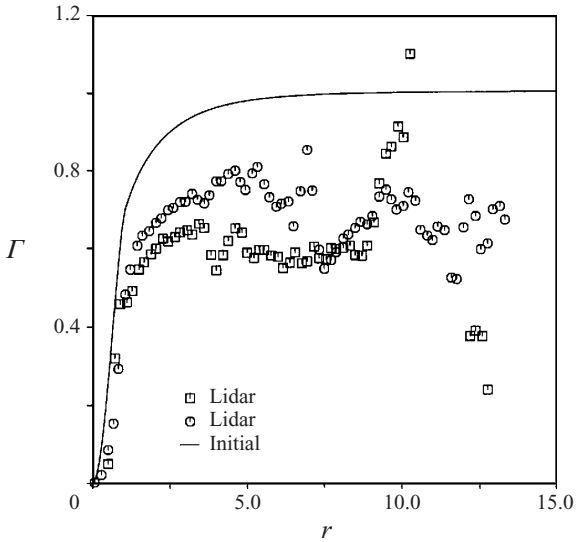


FIGURE 17. Flight measurements of circulation as a function of radial distance in a trailing vortex. The initial profile is given by the solid line. The two sets of symbols correspond to two sets of measurements after a lapse time of 55 s.

flow. One of the viable options for studying vortex decay in high Reynolds number wake flow is the Reynolds-averaged Navier–Stokes approach. Previous calculations (Zeman 1994) of the trailing vortex problem using inadequate pressure–strain correlation models (Zeman & Tennekes 1975) exhibit no discernible decay of the trailing vortex, contrary to observed data. In the absence of more sophisticated pressure–strain correlation models, the Reynolds stress closure methodology as a whole is of little use for studying the trailing vortex problem.

Any turbulence model incapable of predicting elliptic flows will fail in capturing the behaviour of trailing vortex in the wake of aircrafts. The success of the present model in elliptic flows has led to its use in the investigation of the decay mechanisms in trailing vortices. As a first step, Wallin & Girimaji (2000) and Girimaji & Wallin (2000)

https://doi.org/10.1017/S0022112000001336 Published online by Cambridge University Press

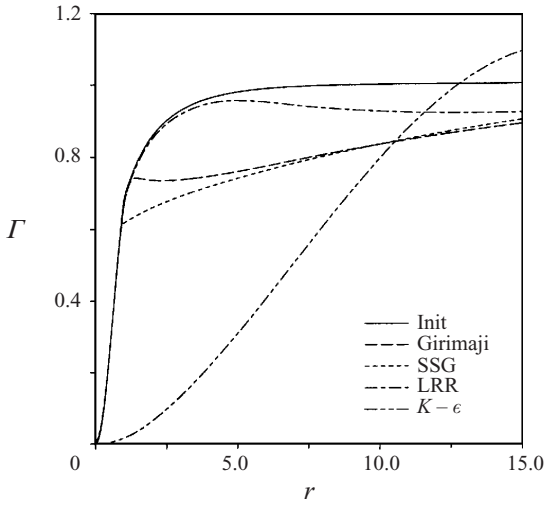


FIGURE 18. Model calculations of circulation as a function of radial distance in a trailing vortex. Different lines correspond to different model calculations after a lapse time of 55 s.

study the two-dimensional decay mechanisms of turbulent vortices. They consider the decay of an axisymmetric turbulent vortex under the influence of turbulent diffusion and Rayleigh instability. This study is restricted to examining curvature effects on turbulence; the elliptic flow instability is not considered. We now present an important result (taken from Wallin & Girimaji 2000) in this turbulent diffusion-dominated flow. In figure 17, a typical initial circulation (Γ) profile of a trailing vortex is given as a function of radius. Also given are two sets of measured profiles (from flight experiments) after a lapse of 55 s. Circulation profiles calculated from four different turbulence models are shown in figure 18. The K–ε model predicts an unphysical overshoot of circulation and a far too rapid decay of the vortex core. The LRR Reynolds stress closure model result shows an overly persistent vortex. This is consistent with the LRR model's general propensity to perform poorly in curved and rotating flows. The SSG model and the present model are most consistent with the measured data. The difference between the SSG and the present models is revealed when dual vortex decay is considered. In this case, each vortex decays in a mean strain field created by the presence of the other vortex. Preliminary calculations have shown that, as expected, the SSG model fails to capture the vortex decay in a mean-strain field correctly whereas the present model does.

Further tests of the present model in practical inhomogeneous flows are currently underway.

7. Summary and conclusion

The objective of this article is to establish and exploit the complete realm of applicability of the standard form of the pressure–strain correlation model. The full potential of the standard form of the model can be realized only if the coefficients are variable functions of the applied mean deformation and the state of turbulence. A methodology for deriving such a model in a rational manner is outlined and implemented. The ensuing pressure–strain model extends the applicability of the standard (LRR) class of models to complex flows – such as vorticity-dominated

https://doi.org/10.1017/S0022112000001336 Published online by Cambridge University Press

elliptic flows and non-equilibrium flows – with minimal *ad hoc* modifications. The study is performed in homogeneous turbulence with two-dimensional mean flows. The methodology, the techniques and the model developed are expected to be useful for three-dimensional mean flows and inhomogeneous turbulence.

The methodology is based on the premise that the extreme states of turbulence – rapid distortion and equilibrium limits – are more amenable to mathematically rigorous modelling since they permit special simplifications not possible at other states. Separate pressure–strain correlation models are developed for the two extreme states. It is not unreasonable to expect that the two models together contain much of the physics relevant to intermediate states of turbulence. The models for the intermediate states are then derived by suitable interpolation.

In the equilibrium state, the turbulence evolves in a self-similar manner so that the Reynolds stress anisotropy (b_{ij}) and timescale ratio ($\omega = \varepsilon/SK$) attain a steady state. The causal relationship between the model's coefficients and its equilibrium behaviour is established by performing fixed point and bifurcation analyses. The model coefficients are specified by requiring that the model bifurcation behaviour be consistent with that of the physical system. The long-time behaviour of the physical system is inferred from the DNS and linear stability results of Blaisdell & Shariff (1996). The equilibrium model coefficients can be scalar functions of the applied mean deformation only.

In the rapid distortion limit, the model coefficients are determined by requiring consistency with the Crow constraint (Crow 1968). For intermediate states of turbulence, the model coefficients are obtained by interpolation between the equilibrium and rapid-distortion states:

$$C_\alpha(\omega) = C_\alpha^{rd} - (C_\alpha^{rd} - C_\alpha^{eq})\, f(\omega/\omega^0). \tag{72}$$

In the above equation, the superscripts *rd* and *eq* indicate the coefficient values in the rapid-distortion and equilibrium limits, ω^0 is the equilibrium value of the timescale ratio and $f()$ is a monotonic function going from zero in the rapid distortion limit to unity in the equilibrium state. It should be emphasized here that the values of the coefficients suggested (equation (67)) are subject to change as our knowledge of the equilibrium state of turbulence improves and more sophisticated one-point closure results become available at the rapid distortion limit.

A list of scalar invariants suitable for use as interpolation parameters in intermediate states of turbulence is compiled. These interpolation parameters depend on the state of the turbulence. Exclusive dependence on the mean deformation invariants is deemed unphysical. From the list of possible interpolation parameters, for the sake of simplicity, we only use the timescale ratio (ω).

The new pressure–strain model, along with the SSG model, is tested against DNS, LES and RDT data for three complex flows: the elliptic streamline flow, rotating shear flow and rapidly distorted flow. The present model captures the growth of kinetic energy and dissipation very well in elliptic flows, whereas the SSG model fails to capture even the qualitative features of the data. The SSG model is well-suited for rotating shear flows to which it is calibrated. The new model and SSG model yield nearly identical results in rotating flows for energetic as well as decaying turbulence cases. In rapidly distorted plane shear and strain turbulence, the new model again does an excellent job of predicting the kinetic energy evolution. The new model simplifies to the SSG model in strain-dominated near-equilibrium flows, thus preserving good agreement in standard benchmark flows in which the SSG model has proved so successful.

https://doi.org/10.1017/S0022112000001336 Published online by Cambridge University Press

In conclusion, a rational methodology for deriving a variable-coefficient pressure–strain model is developed. The resulting model extends the applicability of the standard model form to a wider class of complex flows. While the pressure–strain models still have many obstacles to overcome, the present results indicate reason for optimism. The procedure developed in this paper can also be used to develop a variable-coefficient dissipation model equation of the standard form.

The author would like to thank Professor G. Blaisdell of Purdue University for providing some unpublished data of elliptic flows. The author would also like to thank the late Professor Charles Speziale of Boston University for providing the data used in figures 16 and 17. This research was supported by the National Aeronautics and Space Administration under NASA Contract No. NAS1-19480 while the author was in residence at the Institute for Computer Applications in Science and Engineering (ICASE), NASA Langley Research Center, Hampton, VA 23681-0001.

REFERENCES

Abid, R. & Speziale, C. G. 1993 Predicting equilibrium states with Reynolds stress closure in channel and homogeneous shear flows. *Phys. Fluids* A **5**, 1776–1782.

Bardina, J., Ferziger, J. H. & Reynolds, W. C. 1983 Improved turbulence models based on large eddy simulation of homogeneous, incompressible turbulent flows. *Stanford University Tech. Rep.* TF-19.

Blaisdell, G. A. & Shariff, K. 1996 Simulation and modelling of elliptic streamline flow. *Center for Turbulence Research, Proc. Summer Program 1996.*

Crow, S. 1968 Viscoelastic properties of fine-grained turbulence. *J. Fluid Mech.* **33**, 1–20.

Girimaji, S. S. 1996 Fully explicit and self-consistent algebraic Reynolds stress model. *Theoret. Comput. Fluid Dyn.* **8**, 387–402.

Girimaji, S. S. & Wallin, S. 2000 Study of trailing vortex demise mechanisms using Reynolds stress closure models. *AIAA J.* (submitted).

Johnston, J. P., Haleen, R. M. & Lezius, J. K. 1972 Effects of spanwise rotation on the structure of two-dimensional fully-developed turbulent channel flow. *J. Fluid Mech.* **56**, 533–557.

Kassinos, S. C. & Reynolds, W. C. 1994 A structure-based model for rapid distortion of homogeneous turbulence. *Stanford Mechanical Engineering Department Rep.* TF-61.

Launder, B. E., Reece, G. J. & Rodi, W. 1975 Progress in the development of Reynolds stress turbulence closure. *J. Fluid Mech.* **68**, 537–566.

Lee, M. J. & Reynolds, W. C. 1985 Numerical experiments on the structure of homogeneous turbulence. *Stanford University Tech. Rep.* TF-24.

Pope, S. B. 1975 A more general effective viscosity hypothesis. *J. Fluid Mech.* **72**, 331–340.

Ristorcelli, J. R., Lumley, J. L. & Abid, R. 1995 A rapid-pressure covariance representation consistent with the Taylor-Proudman theorem materially frame indifferent in two-dimensional limit. *J. Fluid Mech.* **298**, 211–248.

Rivlin, R. S. 1957 The relationship between the flow of non-Newtonian fluids and turbulent Newtonian fluids. *Q. Appl. Maths* **15**, 212–215.

Speziale, C. G., Abid, R. & Blaisdell, G. A. 1996 On the consistency of Reynolds stress turbulence closures with hydrodynamic stability theory. *Phys. Fluids* **8**, 781–788.

Speziale, C. G. & Mac Giolla Mhuiris, N. 1989 On the prediction of the equilibrium states in homogeneous turbulence. *J. Fluid Mech.* **209**, 591–615.

Speziale, C. G. & Mac Giolla Mhuiris, N. 1990 Scaling laws for homogeneous turbulent shear flows in a rotating frame. *Phys. Fluids* A **1**, 294–301.

Speziale, C. G., Sarkar, S. & Gatski, T. B. 1991 Modeling the pressure–strain correlation of turbulence: an invariant dynamical system approach. *J. Fluid Mech.* **227**, 245–272.

Thangam, S., Wang, X. & Girimaji, S. S. 1998 Application of a new pressure–strain correlation model to complex flows. *Am. Phys. Soc. (DFD) Bull.* **43**, 2039.

Van Slooten, P. R. & Pope, S. B. 1997 PDF modelling for inhomogeneous turbulence with exact representation of rapid distortions. *Phys. Fluids* **9** 1085–1105.

https://doi.org/10.1017/S0022112000001336 Published online by Cambridge University Press

Wallin, S. & Girimaji, S. S. 2000 Evolution of an isolated trailing vortex. *AIAA J.* (to appear).
Zeman, O. 1994 Persistence of trailing vortices: A modelling study. *Phys. Fluids* **7** 135–139.
Zeman, O. & Tennekes, H. 1975 A self-contained model for the pressure terms in the turbulent stress equation. *J. Atmos. Sci.* **32**, 1808.

https://doi.org/10.1017/S0022112000001336 Published online by Cambridge University Press